

3D PRINTED MICROFLUIDIC DEVICE
FOR POINT-OF-CARE ANEMIA DIAGNOSIS

by

KIMBERLY PLEVNIAK

B.S., University of Kansas, 2014

A THESIS

Submitted in partial fulfillment of the requirements for the degree

MASTER OF SCIENCE

Department of Biological and Agricultural Engineering
College of Engineering

KANSAS STATE UNIVERSITY
Manhattan, Kansas

2016

Approved by:

Major Professor
Mei He

Copyright

KIMBERLY PLEVNIAK

2016

Abstract

Anemia affects about 25% of the world's population and causes roughly 8% of all disability cases. The development of an affordable point-of-care (POC) device for detecting anemia could be a significant for individuals in underdeveloped countries trying to manage their anemia. The objective of this study was to design and fabricate a 3D printed, low cost microfluidic mixing chip that could be used for the diagnosis of anemia.

Microfluidic mixing chips use capillary flow to move fluids without the aid of external power. With new developments in 3D printing technology, microfluidic devices can be fabricated quickly and inexpensively. This study designed and demonstrated a passive microfluidic mixing chip that used capillary force to mix blood and a hemoglobin detecting assay.

A 3D computational fluid dynamic simulation model of the chip design showed 96% efficiency when mixing two fluids. The mixing chip was fabricated using a desktop 3D printer in one hour for less than \$0.50. Blood samples used for the clinical validation were provided by The University of Kansas Medical Center Biospecimen Repository. During clinical validation, RGB (red, green, blue) values of the hemoglobin detection assay color change within the chip showed consistent and repeatable results, indicating the chip design works efficiently as a passive mixing device. The anemia detection assay tended to overestimate hemoglobin levels at lower values while underestimating them in higher values, showing the assay needs to go through more troubleshooting.

Table of Contents

List of Figures	vi
List of Tables	vii
Acknowledgements.....	viii
Chapter 1 - Introduction.....	1
Point-of-Care Diagnostics.....	1
Point-of-Care Microfluidic Device Fabrication.....	1
PDMS.....	2
Glass.....	2
Paper	3
3D Printing.....	4
Anemia.....	5
Point-of-Care Diagnosis and Anemia	8
Objectives	9
References.....	9
Chapter 2 - 3D POC Device Design Theory and Principles.....	16
Calculation Theory	16
Theoretical Design.....	19
Results.....	20
3D Microfluidic Simulation	20
References.....	23
Chapter 3 - Methods and Materials.....	26
Materials	26
Materials used in this project include Visijet FTX clear resin from D3 technologies, and potassium hydroxide (KOH), ethylene glycol, 3,3',5,5'-tetramethylbenzidine (TMB), hydrogen peroxide (H ₂ O ₂) from Sigma Aldrich.....	26
Chip Fabrication.....	26
Assay Optimization.....	27
ImageJ	28
References.....	28

Chapter 4 - 3D Fabrication of Anemia Diagnostic Chip	29
Computer-Aided 3D Design	29
Chip Fabrication	32
References	33
Chapter 5 - Anemia Diagnostic Assay Development	34
Introduction.....	34
Tetramethylbenzidine Oxidation Reaction	34
Optimization Methods	35
Results/Discussion	36
Blood Hemoglobin Assay Optimization.....	38
References.....	39
Chapter 6 - Clinical Validation	41
Laboratory Facilities	41
Clinical Samples	41
Testing Procedures.....	43
Test Tubes	43
Mixing Chips	44
Data Analysis	44
Color Analysis	44
Statistical Analysis.....	48
Linear Regression	48
Bland-Altman Plot	51
References.....	55
Chapter 7 - Conclusions.....	57
Appendix A - Digital Images of Assay Color Change Reactions.....	59
Appendix B - ImageJ RGB Histograms.....	63

List of Figures

Figure 1. Chip A mixing simulation	22
Figure 2. Incomplete mixing of Chip A.....	22
Figure 3. Chip B mixing simulation	23
Figure 4. 2D representation of Chip B.....	30
Figure 5. 3D representation of Chip B.....	30
Figure 6. Chip B outline.....	31
Figure 7. Chip B design	31
Figure 8. 3,5,3,'5'-Tetramethylbenzidine oxidation reaction	35
Figure 9. Hemoglobin powder assay optimization	36
Figure 10. Hemoglobin powder assay optimization	37
Figure 11. Complete mixing of hemoglobin powder.....	38
Figure 12. Assay Optimization	39
Figure 13. Hemoglobin Histograms.....	43
Figure 14. Histograms from ImageJ.	45
Figure 15. Column chart of red color means.	47
Figure 16. Column chart of green color means.....	47
Figure 17. Column chart of blue color means.....	48
Figure 18. Bland-Altman plot.....	52
Figure 19. Bland-Altman plot.	53
Figure 20. Column chart of known hemoglobin levels.....	54
Figure 21. Column chart of known hemoglobin levels.....	54

List of Tables

Table 1. Hemoglobin levels	8
Table 2. Chip A parameters	21
Table 3. Hemoglobin counts	42
Table 4. ImageJ RGB values.	45
Table 5. ImageJ RGB values.	46
Table 6. ImageJ RGB values.	46
Table 7. Regression analysis coefficients.	49
Table 8. Predicted hemoglobin levels.	49
Table 9. Regression statistics.....	50

Acknowledgements

I would like to thank Matthew Campbell for working on the COMSOL simulation and results and I would also like to thank Timothy Myers and Abby Hodges from MidAmerica Nazarene University for their assistance with the hydrophilic channel treatment.

Chapter 1 - Introduction

Point-of-Care Diagnostics

Point-of-care (POC) diagnostic tests can be performed at any location where patient care is provided and do not require trained technicians or a clinical laboratory [1]. A POC test consists of a simple device to operate at low-cost, which shows self-addressable results and interpretations for disease diagnosis, such as viewing a stripe, spot colors, or screen display [1-9]. Each test is usually a single use, disposable device that costs significantly less than conventional laboratory testing. Examples of simple-to-use POC tests include pregnancy, blood glucose, and human immunodeficiency virus (HIV) tests.

The continued development of POC diagnostics is important in healthcare due to several advantages POC tests have over a clinical laboratory, including in-field detection, rapid test results, no facility required, and reduced cost [10-16]. Patients may perform POC tests themselves in the home, allowing them to monitor and manage their own health conditions with reduced medical travel expenses and time [1, 17].

Point-of-Care Microfluidic Device Fabrication

Microfluidics has been a significant area in developing new POC devices. Micropumps and microvalves in microfluidic devices enable precision in sample control and reagent delivery. The three types of materials most commonly used for fabricating microfluidics are polydimethylsiloxane (PDMS), glass, and paper. These materials have been used over the years and each have their own advantages and disadvantages.

PDMS

PDMS has been one of the most used and developed polymers in the area of microfluidics [18]. The wide range of physical and chemical advantages PDMS offers makes it a desirable material to work with. The most significant advantage of PDMS is a wide variety of surface properties [2], which allow modification for meeting fluidic flow and assay requirements [19, 20]. The hydrophobic nature of PDMS allows for resistance to protein and diatom adsorption, which essentially resists to the buildup of molecules on the surface. This is an important factor when picking a material for developing microfluidic devices.

The fabrication of PDMS microfluidic devices is not quick. The entire process takes about a day and must be done in a clean room. PDMS-based microfluidic devices are fabricated using a microscale molding process. The PDMS chip is designed using computer aided design (CAD) and then printed onto a transparency. The transparency acts as a photomask for contact photolithography to transfer the design onto an epoxy-based (SU-8) negative photoresist coated surface of the master mold, which is typically a silicon (Si) wafer. Removal of the unpolymerized photoresist produces a positive relief creating the master mold. The prepolymer of PDMS is then poured into the mold and cured in an oven at 60°C for one hour. The polymer layer is then peeled off and pasted onto a flat plate, which is either polymethylmethacrylate (PMMA) or glass [21-25].

Glass

The use of glass in the fabrication of microfluidic devices is a costly process, requiring trained individuals and expensive equipment. Despite the costly fabrication process, glass

has many properties that are desirable in making microfluidic devices, including stability, optical transparency, and good metal depositions [26, 27]. A few different methods are available to pattern microfluidic channels into glass, including dry/wet etching, photolithography, and electron beam lithography. All of these methods require the use of a clean room [28, 29]. The patterning process involves masking the glass with a metal layer (e.g., gold) that is sputtered using expensive deposition machine and coated with photoresist. The light exposed photoresist and metal layers are then etched away to expose glass for hydrofluoric acid etching [26], which is tedious and labor-intensive work handling hazardous chemicals.

Paper

Many different types of paper microfluidic diagnostic tests, such as the pregnancy test, have been developed and brought to market. Using paper as a microfluidic device is competitive in the field of diagnostic technology due to the ultra-low cost, easy fabrication, short test times, and compatibility with existing benchtop assays in terms of sensitivity [30]. Paper made from 100% cotton is more desirable for diagnostic microfluidic devices because it is cheaper to manufacture than paper made from wood. Most studies on paper-based microfluidics are based on chromatography and filter paper. Important parameters for paper-based microfluidic devices include surface area, capillary flow, pore size distribution, porosity, and color [31].

Wax printing is a commonly used method to produce paper microfluidic devices due to its low cost and simple fabrication of hydrophobic barriers. Modeling software allows the wax

design to be patterned and printed onto the paper. Wax devices are printed by dispensing melted wax as liquid droplets that solidify on the surface of the paper. After printing, the paper is placed on a hotplate where the wax is melted into the paper to create the hydrophobic channels [32, 33]. This method of fabricating paper microfluidic devices is great for making prototypes due to a quick fabrication time of around 5 minutes.

With quick fabrication time and the ability to attach many different assays, paper microfluidic devices have been a popular topic of microfluidic research. The main disadvantage of paper microfluidic devices is that they tend to be temperature and moisture sensitive. Due to these sensitivities, it is hard to store and ship paper-based test devices to underdeveloped countries as a form of POC testing.

3D Printing

With new developments in three-dimensional (3D) printing technology, microfluidic devices can be made with a single piece of equipment, without the need for multiple fabrication steps. Unlike glass, paper, and wax fabrication methods, which produce two-dimensional channels, a 3D printer lays down multiple layers to create three-dimensional channels [34]. The printing process begins with the design and modelling of a microfluidic chip using CAD engineering software. The software design is uploaded into a 3D printer where the microfluidic device is produced. One of the most commonly used fabrication techniques for 3D printing is stereolithographic (SLA), [35,36]. SLA printing uses a vat of liquid resin and an ultraviolet light to build 3D printed parts. An ultraviolet (UV) laser

traces the pattern of each layer on the surface of the resin, which is then cured (solidified) to the previously traced pattern.

Most 3D printers for microfluidic fabrication use SLA with a liquid photopolymer resin as the printing material. A resin is a solid or highly viscous substance that is typically convertible into a polymer. Many resins are synthetic but certain resins are plant derived. Synthetic resins for 3D printing are composed of many monomers along with a small amount of photoinitiator.. [37]. A typical resin mixture consists of 45-55% of a diacrylate, 11-21% of a methacrylate, and 2-3% of a photoinitiator. Resin it is considered to be an irritant and slightly toxic due to the photoinitiator. Once the resin is fully cured and solidified, it is no longer considered an irritant or toxic and is safe to handle without the use of gloves.

One of the major advantages of 3D SLA printing is that the resolution is now comparable to that of PDMS microfluidic devices, but is much faster and more cost effective [38]. 3D printing is considered to be a “skill-less” fabrication technique that allows rapid fabrication of microfluidic devices and may replace PDMS as one of the main microfluidic fabrication techniques in the future [39. 40]. 3D printing might allow for easier access to diagnostic devices for anemia in underdeveloped countries due to fast fabrications times and low costs.

Anemia

Anemia is a condition where an individual has below-normal levels of hemoglobin (Hgb) in the blood, which leads to less oxygen carrying capacity. Symptoms of anemia vary and

can include weakness, fatigue, and other health issues [41]. In some cases, anemia can be severe, long lasting, or even fatal. Anemia is frequently caused by nutrient deficiencies, with iron deficiency being the most common. Iron deficiency anemia (IDA) and anemia are often used interchangeably [42].

According to the World Health Organization (WHO), anemia affects about 25% of the world's population and causes roughly 8% of all disability cases. The population mostly effected by anemia is pregnant women and children, who are more at risk in less developed countries. The risk for developing anemia in less developed countries is due to various factors, such as limited access to healthcare services, housing, and food security [43].

The highest prevalence of anemia in both females and males over time has the same top causes: iron deficiency, hookworms, sickle cell disorders, malaria, and other blood disorders [44-48]. Developing countries that have a high prevalence of anemia tend to also have higher severities of anemia due to the increased chances of contact with infectious agents such as hookworms and mosquitoes. Coming into contact with these infectious agents while having anemia can make anemia more severe.

The current gold standard for anemia testing is a complete blood count (CBC), which includes the measurement of red blood cells, white blood cells, hemoglobin, hematocrit, and platelets[49]. A CBC requires the use of a hematology analyzer. The CBC test standard relies on having access to hospitals or clinics with trained medical professionals. In developing countries, quality healthcare accessibility could be burdensome for patients.

Hemoglobin is a protein in red blood cells that carries oxygen throughout the body and is important in helping red blood cells maintain their normal shape. Iron binds to hemoglobin, which is how hemoglobin levels are analyzed when diagnosing iron deficiency anemia. The healthy range for hemoglobin levels vary between sexes and ages. Hemoglobin levels ranges from normal to severe anemia are listed in Table 1 [50].

Current management methods for anemia vary between developing countries and developed countries. In developed countries, an anemic individual is usually started on iron supplements for a few months to see if that increases their iron/hemoglobin levels. In developing countries, WHO provides worldwide anemia surveillance and anemia control interventions [51-54]. These interventions include optimizing nutrition, adding iron supplements, and providing bed nets to protect individuals from catching malaria from mosquitos.

Table 1. Hemoglobin levels for determining anemia*

Population	Anemia Severity	Hemoglobin Levels
Men (15 years of age and above)	Normal	≥ 13.0
	Mild	11.0 – 12.9
	Moderate	8.0 – 10.9
	Severe	< 8.0
Children 5-11 years	Normal	≥ 11.5
	Mild	11.0 – 11.4
	Moderate	8.0 – 10.9
	Severe	< 8.0
Children 12-14 years	Normal	≥ 12.0
	Mild	11.0 – 11.9
	Moderate	8.0 – 10.9
	Severe	< 8.0
Non-pregnant women (15 years of age and above)	Normal	≥ 12.0
	Mild	11.0 – 11.9
	Moderate	8.0 – 10.9
	Severe	< 8.0
Pregnant women	Normal	≥ 11.0
	Mild	10.0 – 10.9
	Moderate	7.0 – 9.9
	Severe	< 7.0
Men (15 years of age and above)	Normal	≥ 13.0
	Mild	11.0 – 12.9
	Moderate	8.0 – 10.9
	Severe	< 8.0

* Adapted from reference 50

Hemoglobin Levels are in grams per deciliter (g/dL)

Point-of-Care Diagnosis and Anemia

Currently there are two types of POC devices available on the market for self-management of anemia, CO-Oximeters and haemoglobinometers. CO-Oximeters use a multiple wavelength optical sensor to noninvasively measure hemoglobin levels [55], and allows for continuous monitoring of hemoglobin levels. Haemoglobinometers provide rapid

measurement of hemoglobin levels by using a single drop of blood, but do not provide continuous hemoglobin level monitoring. Despite the accuracy and portability of CO-Oximeters and haemoglobinometers, these devices are not affordable for underdeveloped countries, and in some cases, the general public. A single POC device usually cost hundreds of dollars and is not able to be used outside of blood collection clinics. The development of an affordable POC device for detecting anemia could bring much needed healthcare to individuals trying to manage their anemia in both underdeveloped and developed countries.

Objectives

The objective of this study was twofold: 1) design and fabricate a 3D printed, low cost microfluidic mixing chip and 2) develop an anemia diagnostic assay for use with the mixing chip. Combined, the mixing chip and assay would act as a proof of concept for a microfluidic POC diagnostic device for anemia.

References

1. Gubala V, Harris LF, Ricco AJ, Tan MX, Williams DE. 2012. Point of Care Diagnostics: Status and Future. *Analytical Chemistry* 84(2):487-515.
2. Schulze H, Giraud G, Crain J, Bachmann TT. 2009. Multiplexed optical pathogen detection with lab-on-a-chip devices. *Journal of Biophotonics* 2(4):199-211
3. Ahn CH, Choi JW, Beaucage G, Nevin JH, Lee JB, Puntambekar A, Lee JY. 2004. Disposable Smart lab on a chip for point-of-care clinical diagnostics. *Proceedings of the Ieee* 92(1):154-173.

4. Tang M, Wang G, Kong S, Ho H. A Review of Biomedical Centrifugal Microfluidic Platforms. *Micromachines*. 2016 FEB 2016;7(2):UNSP 26.
5. Aldridge C, Foster HM, Albonico M, Ame SM, Montresor A. Evaluation of the diagnostic accuracy of the Haemoglobin Colour Scale to detect anaemia in young children attending primary healthcare clinics in Zanzibar. *Trop Med Int Health*. 2012;17(4):423–429.
6. Ingram CF, Lewis SM. Clinical use of WHO haemoglobin colour scale: validation and critique. *J Clin Pathol*. 2000;53(12):933–937.
7. Paddle JJ. Evaluation of the Haemoglobin Colour Scale and comparison with the HemoCue haemoglobin assay. *Bull World Health Organ*. 2002;80(10):813–816.
8. Critchley J, Bates I. Haemoglobin colour scale for anaemia diagnosis where there is no laboratory: a systematic review. *Int J Epidemiol*. 2005;34(6):1425–1434.
9. Guild J. The colorimetric properties of the spectrum. *Philos T R Soc Lond*. 1932;230A:149–187.
10. McPartlin DA, O'Kennedy RJ. Point-of-care diagnostics, a major opportunity for change in traditional diagnostic approaches: potential and limitations. *Expert Review of Molecular Diagnostics*. 2014 NOV 2014;14(8):979-98.
11. Rainey PM, Ulibarri M. Point-of-Care Testing Is Faster Better? *Am J Clin Pathol*. 2014 NOV;142(5):582-3.
12. St John A, Price CP. Existing and Emerging Technologies for Point-of-Care Testing. *The Clinical biochemist.Reviews / Australian Association of Clinical Biochemists*. 2014 2014 Aug;35(3):155-67.

13. Kristinsson G, Shtivelman S, Hom J, Tunik MG. Prevalence of occult anemia in an urban pediatric emergency department: what is our response? *Pediatr Emerg Care*. 2012;28(4):313–315.
14. Larsson A, Greig-Pylypczuk R, Huisman A. The state of point-of-care testing: a european perspective. *Ups J Med Sci*. 2015 MAR;120(1):1-10.
15. McPartlin DA, O'Kennedy RJ. Point-of-care diagnostics, a major opportunity for change in traditional diagnostic approaches: potential and limitations. *Expert Rev Mol Diagn*. 2014 NOV;14(8):979-98.
16. Petryayeva E, Algar WR. Toward point-of-care diagnostics with consumer electronic devices: the expanding role of nanoparticles. *RSC Adv*. 2015;5(28):22256-82.
17. Ng J, Gitlin I, Stroock A, Whitesides G. Components for integrated poly(dimethylsiloxane) microfluidic systems. *Electrophoresis*. 2002 OCT;23(20):3461-73.
18. McDonald JC, Whitesides GM. Poly(dimethylsiloxane) as a material for fabricating microfluidic devices. *Acc Chem Res*. 2002 JUL 2002;35(7):491-9.
19. Zhou J, Ellis AV, Voelcker NH. Recent developments in PDMS surface modification for microfluidic devices. *Electrophoresis*. 2010 JAN 2010;31(1):2-16.
20. Wu Z, Xanthopoulos N, Reymond F, Rossier J, Girault H. Polymer microchips bonded by O₂-plasma activation. *Electrophoresis*. 2002 MAR;23(5):782-90.
21. McDonald JC, Duffy DC, Anderson JR, Chiu DT, Wu HK, Schueller OJA, et al. Fabrication of microfluidic systems in poly(dimethylsiloxane). *Electrophoresis*. 2000 JAN 2000;21(1):27-40.

22. Y. Xia and G. Whitesides, "Soft lithography," *Angew Chem. Int. Ed.*, vol. 37, pp. 550–575, 1998.
23. Lorenz H, Despont M, Fahrni N, Brugger J, Vettiger P, Renaud P. High-aspect-ratio, ultrathick, negative-tone near-UV photoresist and its applications for MEMS. *Sensors and Actuators A-Physical*. 1998 JAN 1;64(1):33-9.
24. AUMILLER G, CHANDROS.EA, TOMLINSON.WJ, WEBER H. Submicrometer Resolution Replication of Relief Patterns for Integrated Optics. *J Appl Phys*. 1974;45(10):4557-62.
25. Fujii T. 2002. PDMS-based microfluidic devices for biomedical applications. *Microelectronic Engineering* 61-2:907-914.
26. Yuen PK, Goral VN. 2012. Low-Cost Rapid Prototyping of Whole-Glass Microfluidic Devices. *Journal of Chemical Education* 89(10):1288-1292.
27. Iliescu C. Microfluidics in glass: Technologies and applications. *Informacije Midem-Journal of Microelectronics Electronic Components and Materials*. 2006 DEC 2006;36(4):204-11.
28. Li XG, Abe T, Liu YX, Esashi M. 2002. Fabrication of high-density electrical feed-throughs by deep-reactive-ion etching of Pyrex glass. *Journal of Microelectromechanical Systems* 11(6):625-630
29. Iliescu C, Taylor H, Avram M, Miao J, Franssila S. A practical guide for the fabrication of microfluidic devices using glass and silicon. *Biomicrofluidics*. 2012 MAR 2012;6(1):016505.
30. Yetisen AK, Akram MS, Lowe CR. 2013. Paper-based microfluidic point-of-care diagnostic devices. *Lab on a Chip* 13(12):2210-2251.

31. J. C. Roberts, *The Chemistry of Paper*, The Royal Society of Chemistry, 1996
32. Carrilho E, Martinez AW, Whitesides GM. 2009. Understanding Wax Printing: A Simple Micropatterning Process for Paper-Based Microfluidics. *Analytical Chemistry* 81(16):7091-7095.
33. Li X, Ballerini DR, Shen W. A perspective on paper-based microfluidics: Current status and future trends. *Biomicrofluidics*. 2012 MAR 2012;6(1):011301.
34. Bhargava KC, Thompson B, Malmstadt N. Discrete elements for 3D microfluidics. *Proc Natl Acad Sci U S A*. 2014 OCT 21 2014;111(42):15013-8.
35. Ho CMB, Sum Huan Ng, Li KHH, Yoon Y. 3D printed microfluidics for biological applications. *Lab on a Chip*. 2015 2015;15(18):3627-37.
36. Ho CMB, Sum Huan N, Li KHH, Yoon Y-J. 2015. 3D printed microfluidics for biological applications. *Lab on a Chip* 15(18):3627-3637.
37. Hribar KC, Soman P, Warner J, Chung P, Chen S. Light-assisted direct-write of 3D functional biomaterials. *Lab on a Chip*. 2014 2014;14(2):268-75.
38. Shallan AI, Smejkal P, Corban M, Guijt RM, Breadmore MC. Cost-Effective Three-Dimensional Printing of Visibly Transparent Microchips within Minutes. *Anal Chem*. 2014 MAR 18;86(6):3124-30.
39. Au AK, Lee W, Folch A. Mail-order microfluidics: evaluation of stereolithography for the production of microfluidic devices. *Lab on a Chip*. 2014;14(7):1294-301.
40. Capretto L, Cheng W, Hill M, Zhang X. Micromixing Within Microfluidic Devices. *Microfluidics: Technologies and Applications*. 2011 2011;304:27-68.
41. Smith R, The clinical and economic burden of anemia. *Am J Manag Care*. 2010;16(Suppl):S59-S66

42. Khambalia A, Zlotkin S. Iron. In: Walker WA, Watkins JB, Duggan C, eds. Nutrition in Pediatrics: Basic Science and Clinical Applications, 4th ed. Hamilton, ON: BC Decker; 2003:83–98.
43. World Health Organization. Health of Indigenous Peoples. World Health Organization 2007; Fact sheet N°326. October 2007.
44. Salem, M, Chernow, B, Burke, R, et al (1991) Bedside diagnostic testing: its accuracy, rapidity, and utility in blood conservation. *JAMA* 266,382-389.
45. Koukounari A, et al. Relationships between anaemia and parasitic infections in Kenyan schoolchildren: a Bayesian hierarchical modelling approach. *Int J Parasitol.* 2008;38(14):1663–1671.
46. Leenstra T, et al. Schistosomiasis japonica, anemia, and iron status in children, adolescents, and young adults in Leyte, Philippines 1. *Am J Clin Nutr.* 2006;83(2):371–379.
47. Isanaka S, et al. Iron deficiency and anemia predict mortality in patients with tuberculosis. *J Nutr.* 2012;142(2):350–357.
48. Thakur N., Chandra J., Pemde H., Singh V. Anemia in severe acute malnutrition. *Nutrition.* 2014;30:440–442.
49. Buttarello M, Plebani M. Automated blood cell counts - State of the art. *Am J Clin Pathol.* 2008 JUL;130(1):104-16.
50. World Health Organization. Haemoglobin concentrations for the diagnosis of anaemia and assesment of severity. [WHO/NMH/NHD/MNM/11.1]. 2011.
51. Iron deficiency anaemia: assessment, prevention and control. A guide for programme managers. Third Edition. Geneva, World Health Organization, 2007

52. World Health Organization. Essential Nutrition Actions: improving maternal, newborn, infant and young child health and nutrition. Geneva, Switzerland: World Health Organization; 2013.
53. World Health Organization (WHO) Iron Deficiency Anaemia: Assessment, Prevention and Control. A Guide for Programme Managers. WHO; Geneva, Switzerland: 2001
54. World Health Organization (WHO) Anaemia.
55. Giraud B, Frasca D, Debaene B, Mimos O. Comparison of haemoglobin measurement methods in the operating theatre. Br J Anaesth. 2013 DEC 2013;111(6):946-

Chapter 2 - 3D POC Device Design Theory and Principles

In microfluidics, mixing is one of the most fundamental challenges due to the tendency of a fluid to exhibit laminar flow at the microscale [1]. The purpose of this chapter is to look at the principles behind mixing at the microscale and discuss the theoretical development of a microfluidic mixing chip.

Calculation Theory

Fluid flow acts differently at the microscale compared to the macroscale. The variance in fluid flows depends on the differences in dominant forces. Therefore, it is important to investigate the flow behavior of micro channels when designing an efficient microfluidic device.

In microfluidics, the dominant factors include laminar flow, diffusion, advection, fluidic resistance, surface area, and surface tension [2]. The parameters used in designing microfluidic chips include the fluid dynamics, gravitational force, and capillary force, which are determined from the Reynolds Number, Bond Number (Eötvös Number), and Young-Laplace Equation, respectively.

The Reynolds number (Re) is the ratio of inertial forces to viscous forces [3]:

$$Re = \frac{\textit{inertial forces}}{\textit{viscous forces}} = \frac{\rho VL}{\mu}$$

Where:

ρ = density of the fluid

V = kinematic viscosity

L = linear dimension

μ = dynamic viscosity of the fluid

A low Reynolds number indicates that the viscous forces are dominant, while a high number indicates that inertial forces play the dominant role. In addition, the Reynolds number indicates whether a flow is turbulent or laminar. $Re < 2300$ is laminar flow, while $Re > 4000$ is turbulent flow. In small microfluidic devices Reynolds numbers are normally < 100 .

The Bond number (Bo) is the ratio between gravitational force and surface tension force [4]:

$$Bo = \frac{\Delta\rho g L^2}{\sigma}$$

Where:

$\Delta\rho$ = difference in density of the two phases

g = gravitational acceleration

L = characteristic length

σ = surface tension

A Bond number < 1 indicates that surface tension dominates, while a value > 1 indicates gravitational forces dominate. Surface tension is the cohesion between liquid molecules

and the liquid/gas interface. Both Reynolds numbers and Bond numbers give good indications of what the driving force is in passive mixing microfluidic devices. In most microfluidic devices with hydraulic diameters less than 1000 microns, surface tension is usually dominant.

Diffusion is the spontaneous movement of particles from an area of high concentration to an area of low concentration that does not require the use of energy. In the absence of turbulent flow, diffusion dominates the mixing of fluids in microfluidic devices. Diffusion also plays a part in mixing in laminar flows. Over time, the average concentration of particles throughout the channel will become constant through diffusion. Advection, the transfer of matter by fluid flow, enhances diffusion. Advection causes an increase in the interfacial area by transporting mixed fluid away from the interface and introducing new non-mixed fluid [5]. This phenomenon vastly increases mixing time as the rate of diffusion increases. At high Reynolds numbers, advection dominates fluid transport, making diffusion negligible. At moderate Reynolds numbers, fluid flow remains laminar and the internal forces become significant as fluid passes through complex channel geometries. Microchannels (<1000 microns) require high velocities (>100 millimeters/second [mm/s]) to produce adequate mixing.

Capillary flow has received a lot of attention in microfluidics because it moves fluids without the aid of external power [6-8], therefore, it is important to understand the physics of capillary flow to properly design a microfluidic-mixing device. A balance between capillary force and viscous drag determines the flow rate of a fluid [9]. The capillary force

is determined by the channel geometry and the water-air surface tension. This force is characterized by the Young-Laplace Equation [10]:

$$\Delta P = \frac{4\sigma}{D}$$

Where:

ΔP = pressure drop

σ = surface tension

D = channel diameter

The pressure drop (ΔP) can also be expressed in the following equation:

$$\Delta P = \frac{64 L V^2}{Re D^2} \rho$$

Where:

ΔP = pressure

Re = Reynolds number

L = wetted length

V = flow velocity (inversely proportional to the wetted length)

ρ = density of fluid

Theoretical Design

One of the main goals of the POC device design was to create a passive microfluidic mixing device using capillary force. Capillary force is the ability of a liquid to flow through a channel without the assistance of external forces. The diameter of the channel, surface tension, and adhesive forces between the liquid and the channel are what move liquids through passive microfluidic mixers that use capillary force.

Microfluidic devices are typically composed of different basic structures in order to achieve mixing. These basic structures include the T- or Y-junctions, pillars, channels, and cavities. Passive micromixers are able to operate and mix efficiently without the aid of a pump. There are many different types of passive mixers, which include distributive mixers, static mixers, T-type/Y-type mixers, and vortex mixers [11]. These types of micromixers use channel geometry to move fluid streams to increase the area of diffusion. Laminar flow is the dominant flow for most microfluidic devices and usually prevents mixing except through diffusion [12-13]. Therefore, the objective of the design process is to create a microfluidic device that induces diffusion to enhance mixing.

A Y-type mixer, that is able to introduce blood and assay reagents at the same time, was selected as the basic structure for the microfluidic mixing chip. The chip inlets protrude out of the chip to make it easier to draw the reagents into the chip via capillary action. To increase the contact surface, rings were added to split the two fluid streams and recombine them to induce mixing. Studies have shown the effectiveness of splitting and recombining fluid flows to enhance diffusion [14-15]. This initial design is designated as Chip A.

Results

3D Microfluidic Simulation

Using a computational simulation during the prototyping stage is an efficient way to identify problems or validate a design prior to fabrication. Chip A's effective capillary-force driven auto-mixing was evaluated using the 3D computational fluid dynamic (CFD)

simulation module in COMSOL Multiphysics®. The program has an integrated user interface designed for cross-disciplinary product development dealing with electrical, mechanical, fluid, and chemical applications. The CFD module can analyze multiple parameters simultaneously and is used for simulating devices and systems involving sophisticated fluid flow models. Add-ons make it possible to import and edit files such as AutoCAD® and SolidWorks® directly within the program.

The Chip A design was imported into the COMSOL Multiphysics® to calculate the relevant parameters associated with the chip. The chip parameters calculated by the simulation are shown in Table 2.

Table 2. Chip A parameters for COMSOL simulation

Channel Diameter	1mm
Length	~30mm
Final Velocity	337 mm/s
Total Flow Rate	265µL/s
Residence Time	0.045s
Reynolds Number (final)	379
Bond Number	0.136

The simulation showed that the Chip A design had a Bond number <1 , indicating that it is capillary force dominant and works as a passive micromixer. The relatively short channel length of the design resulted in a high capillary driven flow rate of 265 microliters/second ($\mu\text{L/s}$). The calculated flow information was then used to provide input parameters for the CFD analysis. The analysis assumes the two fluids enter the Y-junction at half of the calculated velocity. The two-phase (liquid-liquid) CFD analysis introduced blood in one inlet and reagent in the other. Both fluids were assumed to have the same physical properties as water. The level of mixing for the chip was measured at the viewing window after the

flow reached steady state (not varying with time). The value was then averaged over the viewing port volume (~2mm in diameter). The mixing efficiency of the chip was calculated to be 69% mixed once the fluid flow had reached the viewing window. Figure 1 shows the Chip A COMSOL mixing simulation. Figure 2 shows there is incomplete mixing of hemoglobin powder solution and assay on the side of the rings in Chip A,

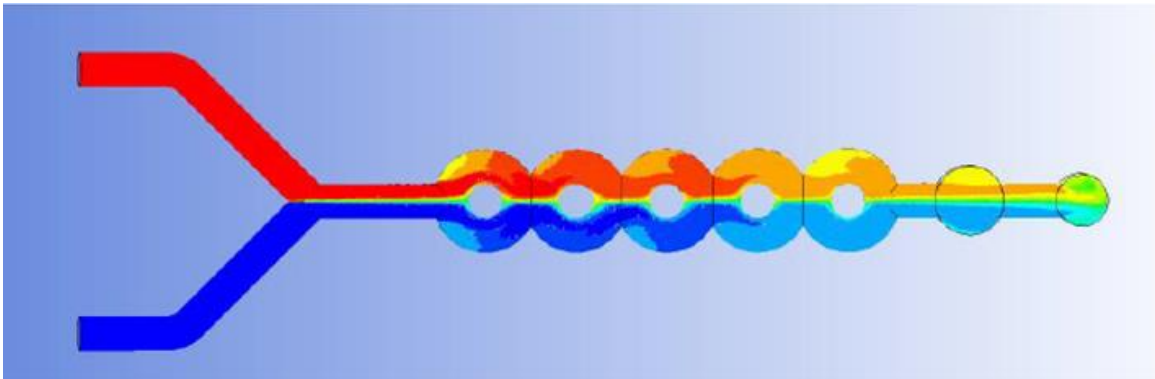


Figure 1. Chip A mixing simulation

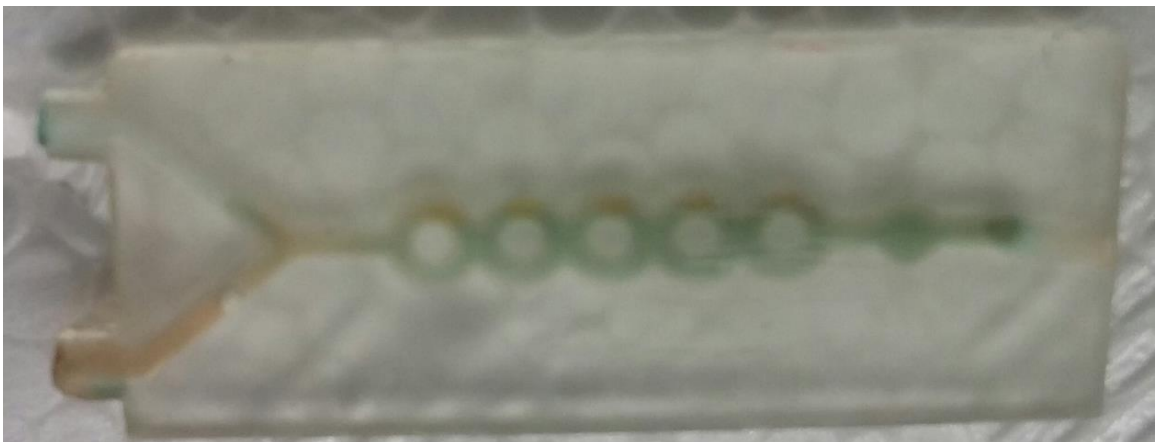


Figure 2. Incomplete mixing hemoglobin powder solution and assay in Chip A

Based on the results of the CFD simulation, the design was modified to rotate the ring portion of the chip 90 degrees to see if the mixing efficiency would increase. A rerun of the

simulation run with the modified design showed a mixing efficiency of 96% mixed once the fluid flow had reached the viewing window as shown in Figure 3.

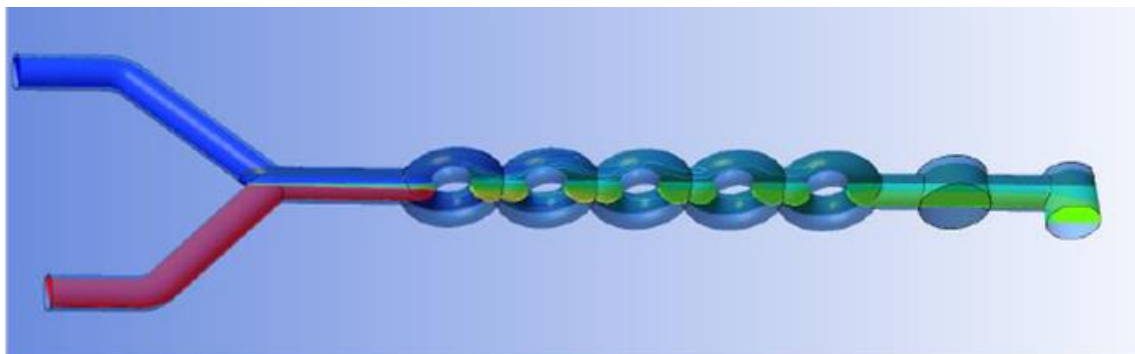


Figure 3. Chip B mixing simulation

The rotation of the ring portion of the chip increased its total thickness, resulting in a decrease in the optical transparency, making the colors harder to see. Therefore, the design was changed to reduce the distance from window to the top of the chip to increase transparency. The modified design, with the ring rotation and changes to the viewing window, was designated as Chip B. The chip parameters from Table 2 are the exact same for Chip B since the design of the chip was not changed, just the orientation of the rings.

References

1. Hashmi A, Xu J. On the Quantification of Mixing in Microfluidics. *Jala*. 2014 OCT 2014;19(5):488-91.
2. Mark D, Haeberle S, Roth G, von Stetten F, Zengerle R. Microfluidic lab-on-a-chip platforms: requirements, characteristics and applications. *Chem Soc Rev*. 2010 2010;39(3):1153-82.

3. Ichikawa N, Hosokawa K, Maeda R. Interface motion of capillary-driven flow in rectangular microchannel. *J Colloid Interface Sci.* 2004 DEC 1 2004;280(1):155-64.
4. Stone HA, Stroock AD, Ajdari A. Engineering flows in small devices: Microfluidics toward a lab-on-a-chip. *Annu Rev Fluid Mech.* 2004 2004;36:381-411.
5. Aubin J, Fletcher DF, Xuereb C. Design of micromixers using CFD modelling. *Chemical Engineering Science.* 2005 APR-MAY 2005;60(8-9):2503-16.
6. C. C. Lai and C. K. Chung, "Numerical simulation of the capillary flow in the meander microchannel," *Microsystem Technologies-Micro-and Nanosystems-Information Storage and Processing Systems*, vol. 19, pp. 379-386, Mar 2013
7. Bertsch A, Heimgartner S, Cousseau P, Renaud P. Static micromixers based on large-scale industrial mixer geometry. *Lab on a Chip.* 2001 2001;1(1):56-60.
8. Mark D, Haeberle S, Roth G, von Stetten F, Zengerle R. Microfluidic lab-on-a-chip platforms: requirements, characteristics and applications. *Chem Soc Rev.* 2010 2010;39(3):1153-82.
9. Zhang J, Yan S, Yuan D, Alici G, Nam-Trung Nguyen, Warkiani ME, et al. Fundamentals and applications of inertial microfluidics: a review. *Lab on a Chip.* 2016 2016;16(1):10-34.
10. Extrand CW. Forces, pressures and energies associated with liquid rising in nonuniform capillary tubes. *J Colloid Interface Sci.* 2015 JUL 15 2015;450:135-40.

11. Beebe DJ, Mensing GA, Walker GM. 2002. Physics and applications of microfluidics in biology. *Annual Review of Biomedical Engineering* 4:261-286.
12. Lee C-Y, Chang C-L, Wang Y-N, Fu L-M. 2011. Microfluidic Mixing: A Review. *International Journal of Molecular Sciences* 12(5):3263-3287
13. Squires TM, Quake SR. Microfluidics: Fluid physics at the nanoliter scale. *Reviews of Modern Physics*. 2005 JUL 2005;77(3):977-1026.
14. Mansur EA, Ye Mingxing, Wang Yundong, Dai Youyuan. A state-of-the-art review of mixing in microfluidic mixers. *Chin J Chem Eng*. 2008 AUG 2008;16(4):503-16.
15. Ansari MA, Kim K, Anwar K, Kim SM. A novel passive micromixer based on unbalanced splits and collisions of fluid streams. *J Micromech Microengineering*. 2010 MAY 2010;20(5):055007.

Chapter 3 - Methods and Materials

Materials

Materials used in this project include Visijet FTX clear resin from D3 technologies, and potassium hydroxide (KOH), ethylene glycol, 3,3',5,5'-tetramethylbenzidine (TMB), hydrogen peroxide (H₂O₂) from Sigma Aldrich.

Chip Fabrication

A 3D representation of the microfluidic device was drawn in AutoCAD[®] using the polyline tool (Figure 4). The channels were drawn using the sweep and extrude tools (Figure 5). A box was then created around the channels using the box tool to create the body of the device (Figure 6). For the last step the subtract tool was used to remove the channels from the box, leaving a hole where the microchannels used to be (Figure 7). The subtract tool is what created the usable microchannels inside of the device. The finished product in Figure 7 is Chip B.

After the design is finished the design is sent to the 3D printer and created.

After the chip was printed, it went through a washing process to remove excess resin from of the chip and out of the channels. The chip was placed in fresh isopropyl alcohol (IPA) for 2 min and then transferred into a container of fresh IPA for another 2 min. After the washing process, the excess resin inside in the channels was blown out using nitrogen gas and was then fully dried. The chip was then placed in the post curing UV chamber for 30 min, where it is allowed to fully cure. Once the chip was post cured, it was treated with a ethylene glycol and 10% potassium hydroxide solution for 1 hour at 55°C to make the chip

more hydrophilic [1]. After treatment, the chip was thoroughly rinsed with water to remove left over ethylene glycol solution and is then dried with nitrogen gas.

Assay Optimization

To create the 8 g/dL solution of hemoglobin powder 3.2mg of hemoglobin powder was inserted into a micro centrifuge tube containing 20 μ L of phosphate buffered saline (PBS). The tube was then vortexed to ensure adequate mixing and then placed on ice. The anemia diagnostic assay consisting of TMB and H₂O₂ was then prepared by adding 3398 μ L of TMB and 2 μ L of H₂O₂. The TMB/H₂O₂ solution was placed on ice after preparation. To test the assay, 50 μ L of the HgB solution (or blood) was diluted in 450 μ L 1x PBS buffer. 50 μ L of the diluted HgB solution was then added to another test tube along with 50 μ L of the TMB/H₂O₂ solution. The combined solutions were then pipetted 5 times to ensure adequate mixing. The reaction was left to sit for 1 min and after that time a digital photo was taken using a LGG3 smartphone. The tests were repeated using 12 g/dL (6 mg HGB powder/ 20 μ L PBS) and 16 g/dL (3.2 mg HGB powder/ 20 μ L PBS).

When the assay was tested on the mixing chip instead of the tubes 50 μ L of the HgB solution (or blood) and TMB/H₂O₂ solution were pipetted onto a PDMS slide. The mixing chip inlets were then touched to both reagents where capillary actions draws in the liquids into the microchannels and mixes them. After 1 min a digital photo of the viewing window was taken using a LGG3 smartphone.

ImageJ

ImageJ was used to analyze the digital photos taken of the chip and tube reactions. The photos were saved as a .JPEG and imported into the software program. The histogram tool was used to analyze the RGB colors of each image and a screenshot of the data was taken and imported into a large spreadsheet for each patient sample for further analysis.

References

1. Kim, R. A. R. Bowen, and R. N. Zare, "Transforming Plastic Surfaces with Electrophilic Backbones from Hydrophobic to Hydrophilic," *ACS Appl Mater Interfaces*, vol. 7, pp. 1925-1931, Jan 28 2015.

Chapter 4 - 3D Fabrication of Anemia Diagnostic Chip

The 3D printer used to fabricate the microfluidic chips is the 3D Systems' Projet 1200®, with a minimum printing resolution of 36µm. Multiple print resolution tests were performed to determine the smallest, working microfluidic channels. Even though the printer resolution is 36µm, channels smaller than 100µm did not form properly or could not be cleared of residue resin after printing. The total thickness of the chip needed to be small enough to allow for the best optical transparency, but large enough for a robust chip. If the chip was too thin, there was risk of blowing out the channels while clearing them with nitrogen gas, creating a hole within the chip. The optimal thickness between the channel and the top of the chip was found to be 250 µm.

Computer-Aided 3D Design

The 3D fabrication design for Chip B was drawn in AutoCAD®. AutoCAD® is a computer software application for 2D and 3D computer-aided design and drafting, which is used across many different industries including architecture, engineering, and graphic design.

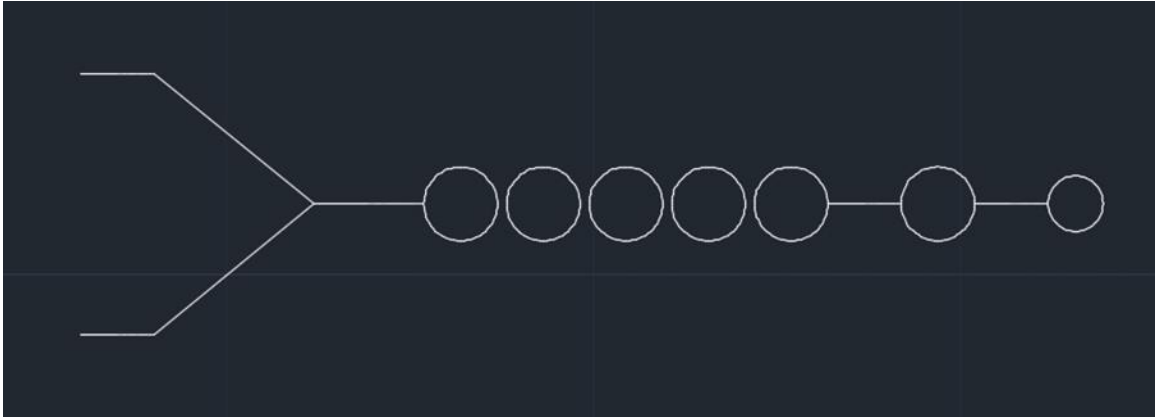


Figure 4. 2D representation of Chip B channels

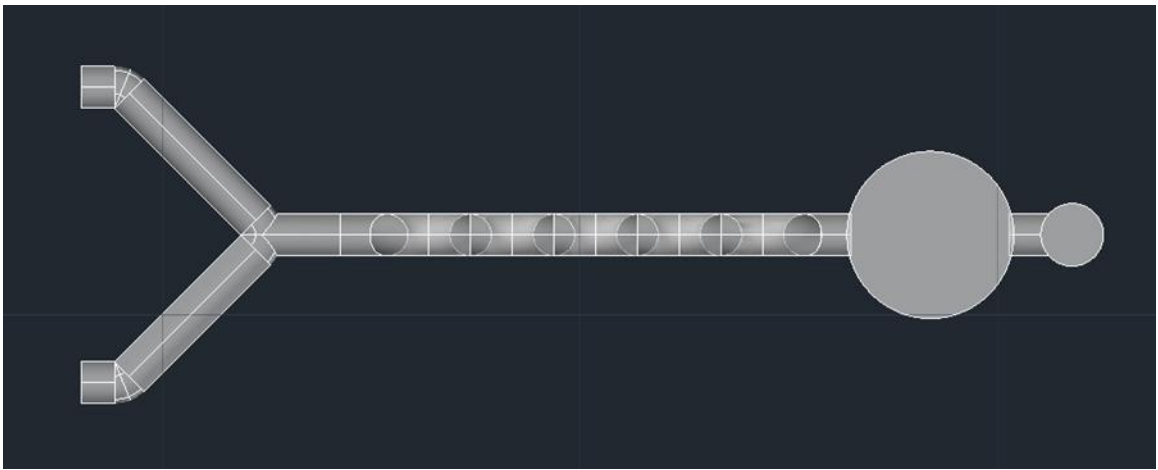


Figure 5. 3D representation of Chip B channels

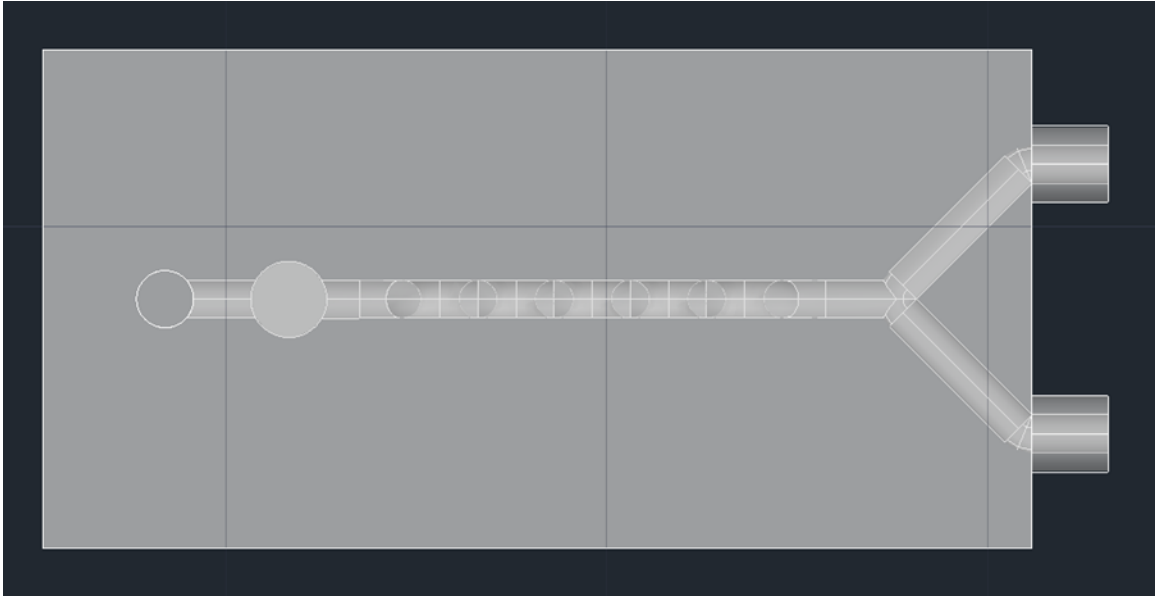


Figure 6. Addition of Chip B outline to channels



Figure 7. Side view of finished Chip B design

After the design was completed, the image was exported and saved as a STereoLithography (.STL) file for use with simulation software and the 3D printer. The .STL file format is the gold standard for transferring data between CAD software and 3D printers. [1] The information from the file is stored in triangulated sections. The more triangles defined on the surface of a file the increased resolution of the printed part [2].

Chip Fabrication

Each chip was fabricated using 3D System's Projet 1200[®]. The Projet is a micro-SLA 3D printer that is compact and easy to use. The printer has a build volume of (43 x 27 x 150 mm) with a resolution of 36 μ m. The printing speed of the Projet 1200[®] is up to 14_{mm/hour}, which allows you to go from design to prototype in just a few hours (in my case only one hour). The fabrication process is quite simple and allows prototyping with ease.

The chip design was uploaded into the printer software as an .STL file and manipulated by adding supports and changing the orientation on the print platform. Adding supports to the chip is necessary to allow the chip to print out properly; otherwise, the chip ends up falling inside of the resin tank. The orientation of the chip on the print platform is important because the chip prints upside-down. Due to this factor, the outlet is the last thing printed so that the microchannels can be cleared of uncured resin.

Once the design file is sent to the printer, the file is 'sliced' within the printer program to determine the layers to be printed. The print platform is then lowered into the resin cartridge and the chip begins to print. A UV light within the printer flashes the design pattern on to the liquid resin for each layer. When the UV light hits the resin, it hardens (cures) the liquid into to a solid. After each layer is printed, the platform slightly raises up and the next layer is printed right on top. When printing, it is important that the printer be kept on a stable surface to avoid shaking. If the printer shakes during printing, it can cause the layers to be misaligned, creating unusable chips.

References

1. Dolenc A, Makela I. Slicing Procedures for Layered Manufacturing Techniques. *Comput -Aided Des.* 1994 FEB 1994;26(2):119-26.
2. Beebe DJ, Mensing GA, Walker GM. 2002. Physics and applications of microfluidics in biology. *Annual Review of Biomedical Engineering* 4:261-286.S.

Chapter 5 - Anemia Diagnostic Assay Development

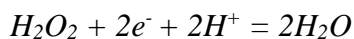
Introduction

An anemia diagnostic assay was developed for use with the microfluidic mixing chip. The goal was to create an assay able to detect differences in hemoglobin levels with a visual color change. The assay was made by mixing 3,5,3',5'-Tetramethylbenzidine (TMB) with hydrogen peroxide (H₂O₂). Benzidines are used as reagents to test for blood due to the peroxidatic activity of blood [1]. This reaction has been used in portable point-of-care photometers for anemia detection and enzyme-linked immunosorbent assay (ELISA) tests.

Tetramethylbenzidine Oxidation Reaction

The reaction between TMB, hemoglobin, and H₂O₂ has been well documented [1-6]. The system yields colored products, which changes from blue, to green, and ending at yellow [7]. The blue product is a one-electron oxidation product of tetramethylbenzidine, while the yellow product is the two-electron oxidation product (diimine). The concentration of the hemoglobin affects the rate of the reaction but not the concentration of the formed product. The relationships between these products can be seen in Figure 8.

During this process, the heme center of the hemoglobin reduces peroxide to water under the equation:



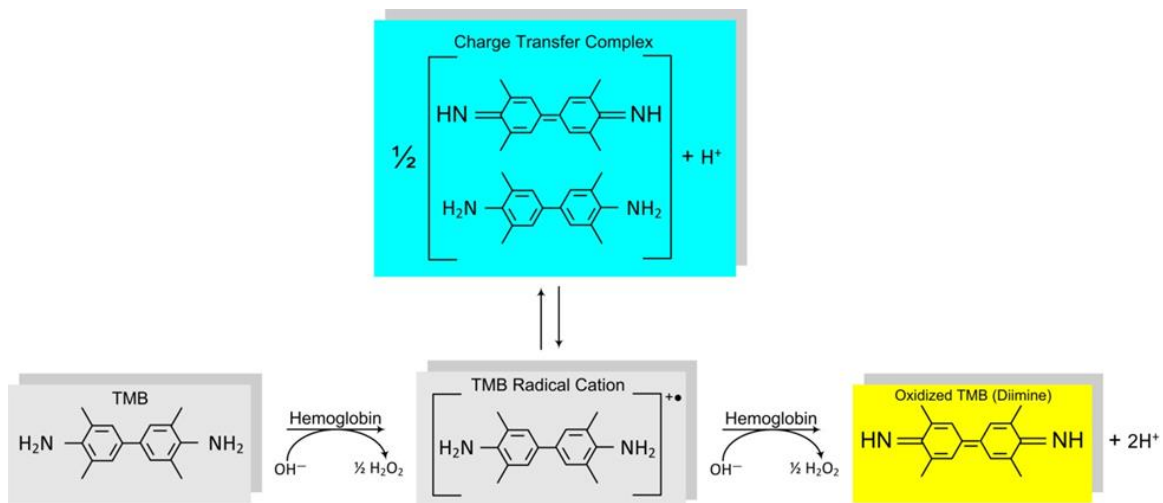


Figure 8. 3,5,3',5'-Tetramethylbenzidine oxidation reaction

The consumption of protons raises the pH of the solution. From previously published literature [1,2], expected color changes should include blue, green, yellow, orange and red, with blue color indicating severe anemia and red indicating no anemia.

Optimization Methods

Before working with human blood, human hemoglobin powder was used to catalyze the reaction between TMB and H_2O_2 in test tubes. After reviewing multiple ELISA substrates containing TMB and H_2O_2 , the recommended ratio was 1:2 or 1:3 ratio [1] of TMB/ H_2O_2 . The initial experiments started with a 1:3 ratio (1650 μM of TMB to 4950 μM of 30% H_2O_2). The hemoglobin powder concentrations used were 8g/dL, 12g/dL, and 16g/dL to simulate severe anemia, mild anemia, and no anemia.

Results/Discussion

The tube reactions gave varying color changes from blue, to yellow/orange, to orange after 1 minute, having colors ranging gave a nice visual correlation between color and hemoglobin counts. The observed results showed the expected color variation for the hemoglobin powder concentrations as shown in Figure 9.



Figure 9. Hemoglobin powder assay optimization in tubes. From left to right: 16 g/dL, 12 g/dL, 8 g/dL.

The colors in the chips came out slightly different from the ones in the tubes as seen in Figure 10. The 8 g/dL was very similar to the tube, but the 16 g/dL turned out to be more of a yellow/green than a yellow/orange. Even though there were slight color differences between the chips and the tubes, the assay optimization established a starting point for use with patient samples. Figure 11 shows complete mixing of hemoglobin powder 8 grams per deciliter (g/dL) and 16 g/dL solution throughout Chip B.

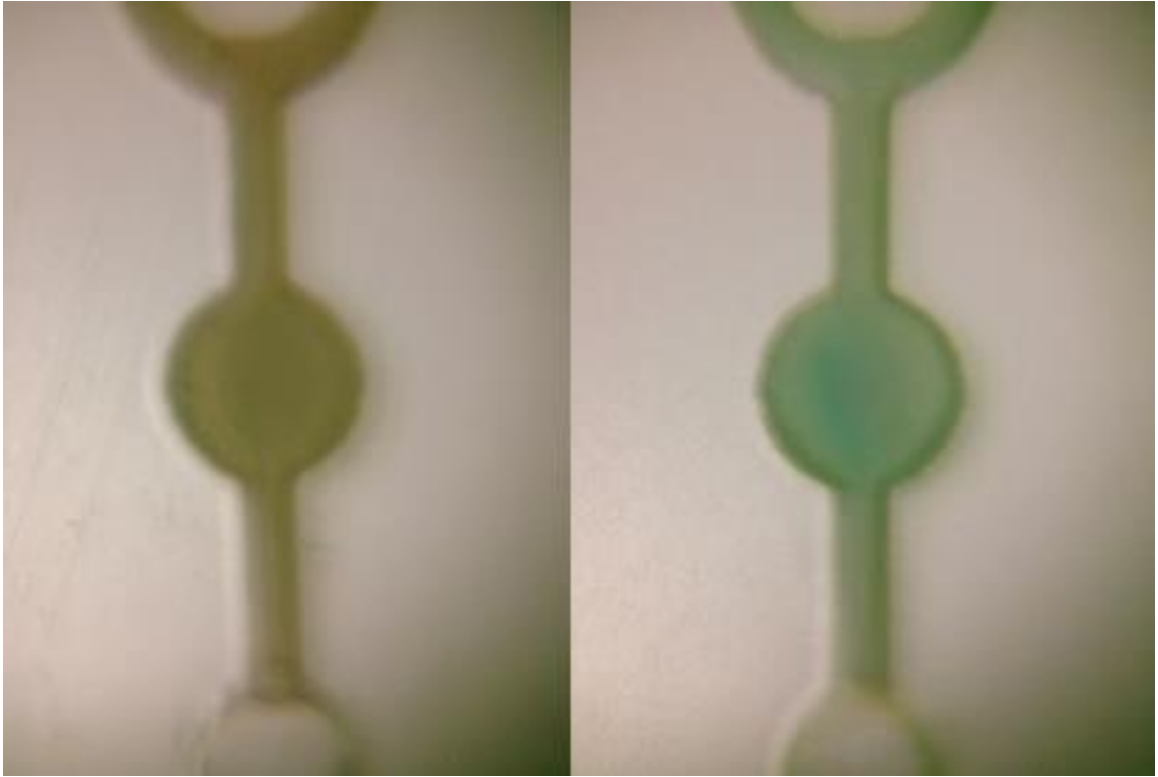


Figure 10. Hemoglobin powder assay optimization in mixing chips (16 g/dL and 8 g/dL)



Figure 11. Complete mixing hemoglobin powder solution and assay in Chip B. (8 g/dL and 16 g/dL)

Blood Hemoglobin Assay Optimization

The anemia detection assay needed to be optimized for the clinical patient blood samples. Initially, anemic blood samples were diluted by 10x, but the dilution was not enough to show the blue charge transfer complex ; the red color of the heme was too intense to show the blue hue. The blood samples were then diluted by 50x and 100x to see if any color changes were visible. The 50x and 100x dilution results can be seen in Figure 12. With these results, it was concluded that the samples needed to be diluted by 100x to see any

color change, since any dilution beyond 100x would produce no visible color change. After the assay was re-optimized for the patient blood samples, the point-of-care microfluidic device was ready for testing.

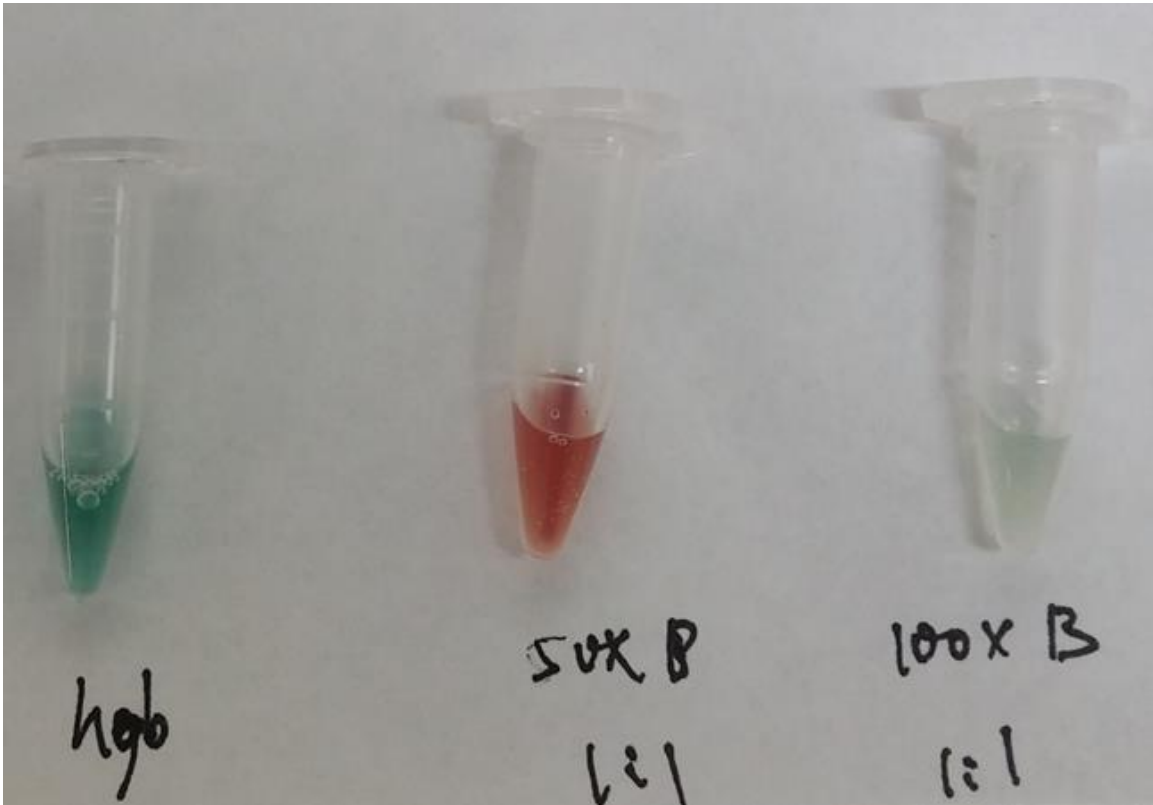


Figure 12. Comparison of HgB powder, anemic patient 50x Dilution, anemic patient 100x assay Optimization

References

1. Josephy PD, Eling T, Mason RP. The Horseradish Peroxidase-Catalyzed Oxidation of 3,5,3',5'-Tetramethylbenzidine - Free-Radical and Charge-Transfer Complex Intermediates. *J Biol Chem.* 1982 1982;257(7):3669-75.
2. Reynolds M, Lawlor E, McCann SR, Temperley IJ. Use of 3,3',5,5'-tetramethylbenzidine (TMB) in the identification of erythroid colonies. *J Clin Pathol.* 1981;34(4):448-449

3. Levinson SS, Goldman J. Measuring hemoglobin in plasma by reaction with tetramethylbenzidine. *Clin Chem.* 1982;28(3):471–474.
4. Zierdt WS, Zierdt CH. Occult blood testing using tetramethylbenzidine in an extraction procedure for patients on unrestricted diets. *Am J Clin Pathol.* 1985;83(4):486–488.
5. Laberke PJ, Hausmann R, Wiprachtiger N, Briellmann T, Balitzki B. [Analysis with the Combur-Test — special aspects in forensic trace examination]. *Arch Kriminol.* 2012;229(5–6):189–197.
6. Laberke PJ, Hausmann R, Wiprachtiger N, Briellmann T, Balitzki B. [Analysis with the Combur-Test — special aspects in forensic trace examination]. *Arch Kriminol.* 2012;229(5–6):189–197.
7. Tyburski EA, Gillespie SE, Stoy WA, Mannino RG, Weiss AJ, Siu AF, et al. Disposable platform provides visual and color-based point-of-care anemia self-testing. *J Clin Invest.* 2014 OCT 2014;124(10):4387-94.

Chapter 6 - Clinical Validation

Laboratory Facilities

Work with human blood poses a moderate health hazard due the potential for exposure to human diseases and infectious organisms. In addition to standard safety practices for Biosafety Level 1 (BSL 1) laboratories, the facility must meet Biosafety Level 2 (BSL 2) standards. These standards include precautions to prevent injury (needle sticks, cuts, ingestion, and mucous membrane exposures), controlled access to the lab, and equipment such biosafety cabinets, personal protective equipment, autoclave, and eyewash station.

To meet BSL-2 standards, a biosafety manual and standard operating procedures were prepared and submitted to the Kansas State University Institutional Biosafety Committee (IBC #1082 and IRB #8032) for review and approval. Approval of the facility as a BSL-2 lab was received prior to receiving and testing clinical samples.

Clinical Samples

Blood samples with hemoglobin counts used for the clinical validation were provided by The University of Kansas Medical Center Biospecimen Repository. Samples were collected from lists healthy and anemic patients within their database, two from non-anemic (normal) patients and 16 from anemic patients. Each sample was preserved in acid citrate dextrose (ACD) anticoagulant and stored at 4°C until pickup. Once the samples were received, they were stored at 4°C, if being used the same day, or at -80°C for later testing. The hemoglobin counts for the clinical samples are listed in Table 3. HgB values ranged from 6g/dL to 14.5g/dL. A histogram (Figure 13) of the data indicates normal distribution

of the data. The exact numbers of the hemoglobin values for each sample were not received until after the study was complete. When samples were received the possible range of the hemoglobin levels was known, but the exact hemoglobin levels for each sample was not known during the time of testing.

Table 3. Hemoglobin counts of patient samples.

Sample Number	Patient Number	HgB
1	15267	6
2	17669	7.3
3	17193	7.5
4	12218	8.3
5	16367	8.5
6	20258	8.6
7	20452	8.8
8	5996	9.5
9	20737	9.6
10	19262	9.7
11	5675	9.7
12	3659	9.8
13	20485	10.1
14	15429	10.1
15	14476	10.2
16	20247	11.7
17	16701	14.1
18	10439	14.5

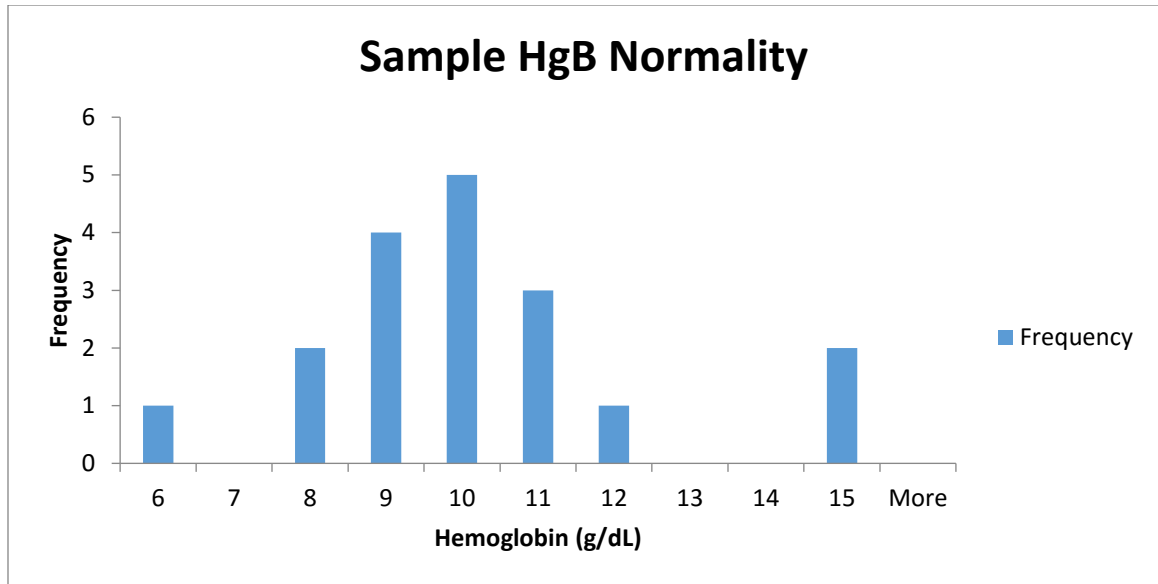


Figure 13. Histogram of hemoglobin ranges of patient samples

Testing Procedures

Test Tubes

Initial testing of hemoglobin levels in patient samples was performed using test tubes to assess the performance of the assay independent of the mixing chips. The test tubes act as a control to ensure proper mixing was achieved when assessing the performance of the assay. The protocols for running the tube samples are as follows:

1. Dilute 5 μ L of blood in 450 μ L 1x PBS solution and put on ice.
2. Add 3498 μ L of TMB and 2 μ L of 30% H₂O₂ and put on ice.
3. Add 50 μ L of blood to the test tube.
4. Add 50 μ L of TMB/H₂O₂ to the test tube.
5. Pipet the mixture 5 time and let reaction sit for 3 minutes.
6. After 3 minutes, a digital photo of the tube is taken.

Mixing Chips

The chip design used for these tests was Chip B. The anemia test was replicated (Chip 1, Chip 2) for each patient sample to assess the mixing efficiency of the chips as well as the accuracy of the assay to predict hemoglobin levels. The mixing chips were prepped for testing by pipetting water into the microchannels to activate hydrophilic treatment. After 2 minutes, the water was vacuumed from the channels. Each TMB/H₂O₂ reaction mixture was made fresh and kept on ice for each test. The blood samples were kept on ice when not in storage. The protocols for running the chip samples are as follows:

1. Dilute 5 μ L of blood in 450 μ L 1x PBS solution and put on ice.
2. Add 3498 μ L of TMB and 2 μ L of 30% H₂O₂ and put on ice.
3. Add 50 μ L of blood to the PDMS slide.
4. Add 50 μ L of TMB/H₂O₂ to the PDMS slide.
5. The mixing chip inlets are then touched to the blood and reagent droplets on the PDMS surface where capillary action draws the liquids into the chip for mixing.
6. After 3 minutes, a digital photo of the mixing chip viewing window is taken .

Data Analysis

Color Analysis

The digital photos taken of the Tube, Chip 1, and Chip 2 color change for each patient sample test were cropped to a 150 x 150 pixel square to keep the image size consistent during color analysis. Copies of the digital photos are provided in Appendix A. The digital images were analyzed using ImageJ®. ImageJ® is an open source image-processing

program that generates an RGB (red, green, blue) histogram along with the mean, mode, minimum, maximum, and standard deviation of the color spectrum. A sample of the ImageJ is presented below as Figure 14. The ImageJ® histograms and color data for each test is included in Appendix B. A summary of the ImageJ® RGB data is presented in Tables 4, 5, and 6.

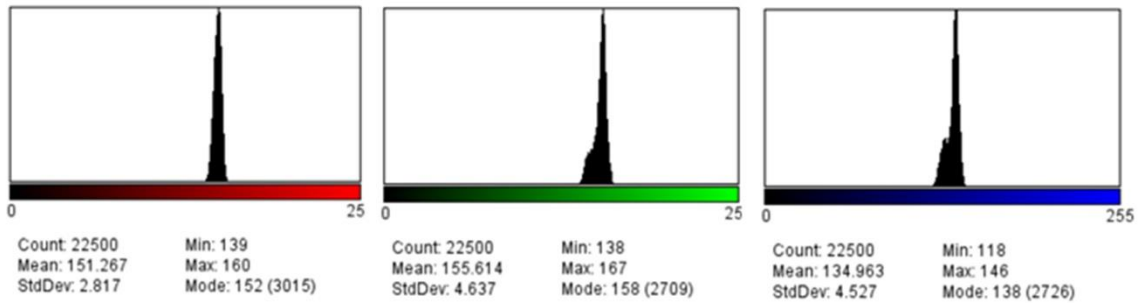


Figure 14. Histograms from ImageJ.

Table 4. ImageJ RGB values from Tube images.

Sample #	Patient #	HgB	R Mean	G Mean	B Mean	R Std Dev	G Std Dev	B Std Dev
1	15267 - Tube	6	163.288	155.614	134.963	4.946	4.637	4.527
2	17669 - Tube	7.3	157.545	151.741	137.108	3.741	3.818	5.07
3	17193 - Tube	7.5	124.197	132.221	116.941	3.841	3.024	2.989
4	12218 - Tube	8.3	140.145	141.864	126.867	2.969	2.662	2.773
5	16367 - Tube	8.5	127.693	132.009	112.003	3.217	2.79	3.965
6	20258 - Tube	8.6	106.44	135.975	114.855	5.135	3.45	4.117
7	20452 - Tube	8.8	128.733	143.034	126.299	4.539	3.975	4.394
8	5996 - Tube	9.5	5.279	86.312	88.304	4.681	4.981	4.853
9	20737 - Tube	9.6	138.662	141.432	125.844	3.359	3.084	3.169
10	19262 - Tube	9.7	109.359	133.157	107.619	13.002	8.958	10.99
11	5675 - Tube	9.7	20.154	105.503	110.278	10.259	6.246	5.557
12	3659 - Tube	9.8	140.131	138.331	120.595	7.728	7.466	5.754
13	20485 - Tube	10.1	118.438	127.527	115.889	8.76	6.51	6.247
14	15429 - Tube	10.1	142.766	149	136.229	6.753	6.551	6.998
15	14476 - Tube	10.2	132.011	125.658	107.353	4.97	4.758	5.103
16	20247 - Tube	11.7	152.937	148.659	121.847	7.718	7.803	9.158
17	16701 - Tube	14.1	130.046	133.682	116.31	4.789	4.181	5.446
18	10439 - Tube	14.5	142.935	142.957	123.043	4.257	3.895	4.369

Table 5. ImageJ RGB values from Chip 1 images.

Sample #	Patient #	HgB	R Mean	G Mean	B Mean	R Std Dev	G Std Dev	B Std Dev
1	15267 - Chip	6	151.267	145.159	133.779	2.817	2.149	2.983
2	17669 - Chip	7.3	160.663	155.989	150.34	2.75	2.624	3.433
3	17193 - Chip	7.5	133.802	138.536	126.547	3.526	2.68	4.484
4	12218 - Chip	8.3	147.631	148.701	141.806	3.314	3.603	4.53
5	16367 - Chip	8.5	158.743	155.962	155.964	2.282	2.417	3.219
6	20258 - Chip	8.6	124.617	135.408	122.46	2.639	2.155	3.323
7	20452 - Chip	8.8	124.954	137.534	125.246	3.132	2.983	4.198
8	5996 - Chip 1	9.5	158.618	140.855	128.835	1.924	1.901	3.001
9	20737 - Chip1	9.6	164.378	157.202	158.9	2.355	3.624	4.956
10	19262 - Chip1	9.7	125.029	144.854	141.295	3.677	2.83	3.553
11	5675 - Chip 1	9.7	145.12	148.231	139.35	2.95	2.563	3.422
12	3659 - Chip 1	9.8	155.358	144.732	133.623	2.131	1.809	2.157
13	20485 - Chip	10.1	155.443	158.936	164.194	3.588	3.596	4.591
14	15429 - Chip1	10.1	163.559	162.73	162.821	4.183	3.693	5.328
15	14476 - Chip	10.2	154.554	145.251	143.921	2.209	3.177	4.586
16	20247 - Chip	11.7	134.291	135.619	128.863	3.727	4.068	5.469
17	16701 - Chip	14.1	150.393	133.019	131.801	2.086	3.49	3.831
18	10439 - Chip	14.5	161.778	154.467	152.336	2.265	2.473	2.884

Table 6. ImageJ RGB values from Chip 2 images.

Sample #	Patient #	HgB	R Mean	G Mean	B Mean	R Std Dev	G Std Dev	B Std Dev
1	15267 - Chip	6	155.489	155.489	140.169	4.665	3.422	5.909
2	17669 - Chip	7.3	154.811	151.668	148.43	2.448	2.12	2.447
3	17193 - Chip2	7.5	163.316	161.297	166.445	1.633	1.539	1.658
4	12218 - Chip	8.3	149.362	149.509	149.53	3.132	3.068	3.079
5	16367 - Chip	8.5	141.507	152.381	152.939	2.954	2.061	2.393
6	20258 - Chip2	8.6	121.787	134.904	122.529	4.895	3.589	4.61
7	20452 - Chip	8.8	138.761	135.087	126.614	4.437	4.383	7.808
8	5996 - Chip 2	9.5	161.181	148.664	142.081	2.364	2.012	2.493
9	20737 - Chip2	9.6	164.306	157.264	158.938	2.614	4.126	5.609
10	19262 - Chip	9.7	110.862	136.774	138.295	13.283	11.04	10.893
11	5675 - Chip2	9.7	144.399	144.495	136.794	3.22	2.772	3.097
12	3659 - Chip 2	9.8	154.942	145.025	135.948	2.77	3.284	5.53
13	20485 - Chip	10.1	163.906	167.585	170.094	3.63	3.728	4.408
14	15429 - Chip	10.1	164.864	162.05	162.823	2.289	2.14	2.95
15	14476 - Chip	10.2	162.758	159.758	158.654	3.484	4.036	5.043
16	20247 Chip 2	11.7	133.823	135.187	128.549	3.998	4.4	6.011
17	16701 - Chip	14.1	162.646	153.345	150.455	2.452	2.58	2.895
18	10439 - Chip	14.5	159.749	146.069	144.501	2.117	2.136	2.605

Column charts (Figures 15, 16, and 17) were generated to compare the RGB value means of Chip 1 and Chip 2 for each sample. The charts show little variance in the RGB means between Chip 1 and Chip 2, indicating repeatability in the mixing between the two chips.

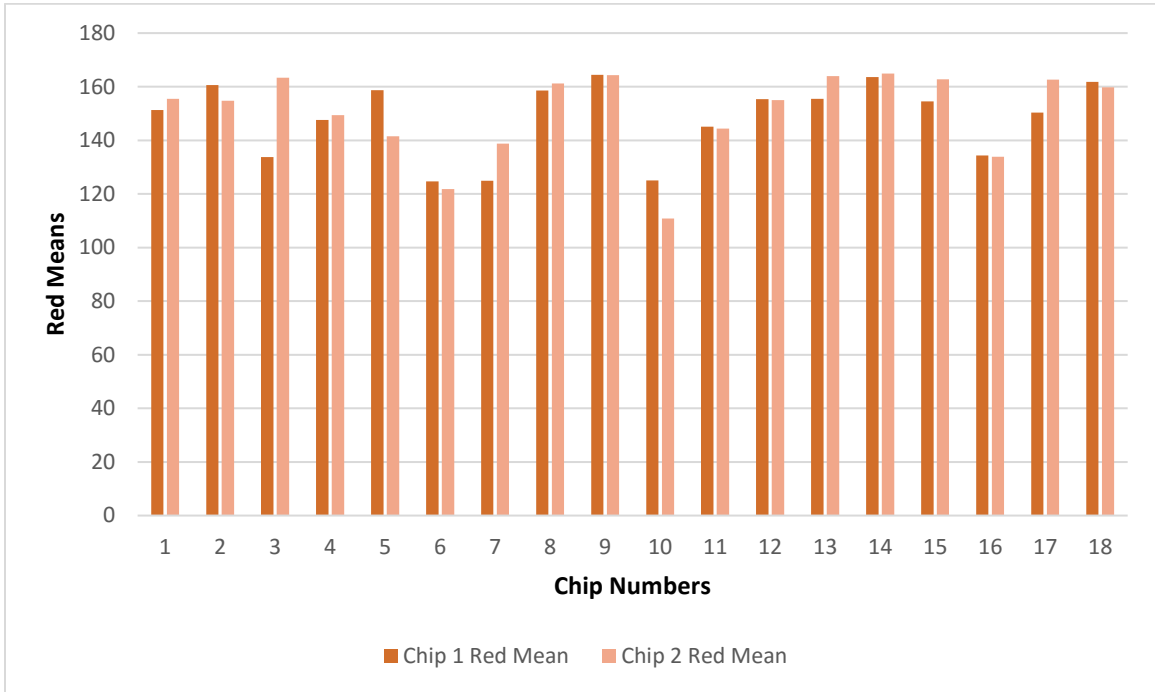


Figure 15. Column chart of Chip 1 and Chip 2 red color means.

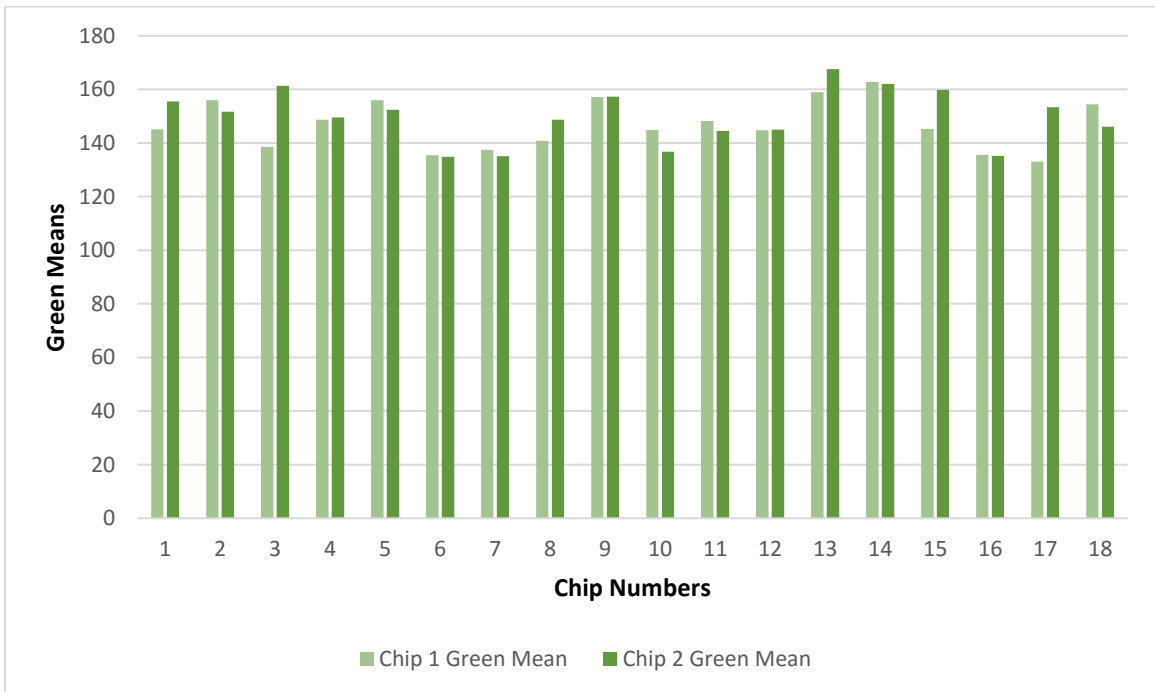


Figure 16. Column chart of Chip 1 and Chip 2 green color means.

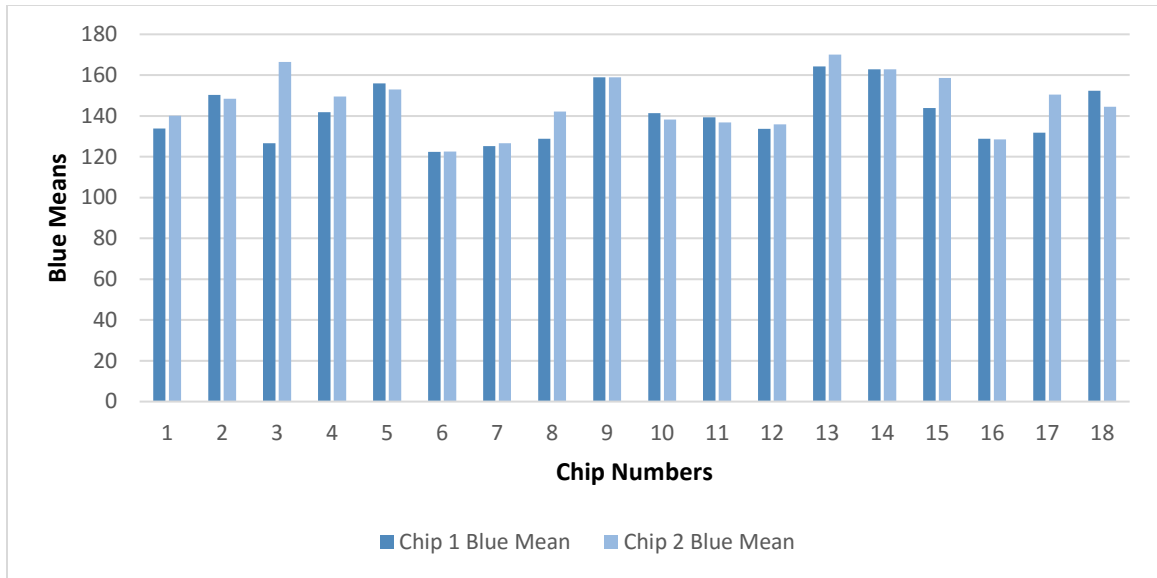


Figure 17. Column chart of Chip 1 and Chip 2 blue color means.

Statistical Analysis

Linear Regression

Linear regression analysis was used to model the relationship between the RGB and clinical HgB values. This type of analysis, also known as predictive analysis, fits the observed data to a linear equation. This equation can then be used to predict a value from the observed data. The prediction equation is:

$$y = \beta_0 + \beta x$$

Where:

β_0 = intercept

βx = is the slope

For three variables (RGB) the prediction equation is:

$$y = \beta_0 + \beta_1 x_1 + \beta_2 x_2 + \beta_3 x_3$$

The regression analysis was performed with Microsoft Excel’s data analysis regression tool using the known HgB values and the measured mean RGB from Chip 1 and Chip 2 for each sample. Table 7 shows the intercept and slopes from the regression analysis.

Table 7. Regression analysis coefficients.

	<i>Coefficients</i>
Intercept	27.80
X Variable 1 (R)	0.085
X Variable 2 (G)	- 0.42
X Variable 3 (B)	0.22

The prediction equation for predicting hemoglobin levels from the RGB numbers is:

$$y = 27.80 + 0.085R + (-0.48)G + 0.22B$$

The known and predicted HgB levels for each sample, along with difference (residual) between the values, are presented in Table 8.

Table 8. Predicted hemoglobin levels using prediction equation.

Sample #	Patient #	Known HgB	Chip 1 HgB	Chip 2 HgB	Tube HgB	Chip 1 Residual	Chip 2 Residual	Tube Residual
1	15267	6	8.4	6.6	9.1	-2.9	-0.3	-3.1
2	17669	7.3	8.5	9.8	8.8	-1.5	-2.5	-1.5
3	17193	7.5	8.7	10.2	9.9	-1.1	-2.9	-2.4
4	12218	8.3	8.9	10.3	9.4	-0.6	-2.2	-1.1
5	16367	8.5	10.1	8.8	10.3	-1.5	-0.8	-1.8
6	20258	8.6	8.5	8.0	9.7	0.4	0.4	-1.1
7	20452	8.8	8.3	10.7	9.2	0.8	-1.7	-0.4
8	5996	9.5	9.4	10.6	10.2	-0.8	-0.6	-0.7
9	20737	9.6	10.6	10.6	9.4	-1.0	-0.9	0.2
10	19262	9.7	9.5	9.0	10.3	1.2	-0.4	-0.6
11	5675	9.7	8.3	9.3	8.7	1.4	0.4	1.0
12	3659	9.8	8.8	10.2	9.9	0.4	0.0	-0.1
13	20485	10.1	10.9	8.3	9.9	-0.2	1.5	0.2
14	15429	10.1	9.0	9.4	8.7	1.1	0.7	1.4
15	14476	10.2	11.6	9.3	10.8	-1.3	0.9	-0.6
16	20247	11.7	10.8	10.5	9.9	1.3	1.2	1.8
17	16701	14.1	13.8	10.4	10.0	0.5	3.9	4.1
18	10439	14.5	9.9	12.0	9.7	4.5	2.8	4.8

How well the data fits a linear relationship is determined by the regression statistics are summarized in Table 8.

Table 9. Regression statistics.

<i>Regression Statistics</i>	
R	0.60
R Square	0.36
Adjusted R Square	0.30
Standard Error	1.75
Observations	36

Where:

Correlation coefficient (R) = strength the linear relationship of the data

Coefficient of determination (R^2) = how many points fall on the regression line

Adjusted R Square = used when there are multiple X values

Standard Error (S) = average distance that the observed values fall from the regression line

An R value of 1 shows a positive correlation between the two sets of data, while a value of 0 shows no relationship. The R value of 0.60 indicates that there is not a strong linear relationship in the data. The adjusted R^2 (for multiple X values) is 0.30, which means 30% of the data fit the model. S indicates how wrong the regression model is on average using the units of the response variable (in this case hemoglobin count). Smaller values are better because it indicates that the observations are closer to the fitted line. This number is saying the average distance of the data points from the plotted line is a hemoglobin count of around 1.75.

The output from the linear regression was used to create a Bland and Altman Plot to show a visual correlation between the known and predicted hemoglobin levels.

Bland-Altman Plot

A Bland Altman Plot is often used by researchers to compare two methods of measurement, or a new method of measurement with an established one, to determine whether these two methods can be used interchangeably or the new method can replace the established one [1-4]. This method calculates the mean difference (bias) between two methods of measurement and the limits of agreement. The limits of agreement is usually 95%, and the mean difference is within 1.96 standard deviations. With these plots, there is a lower limit of agreement and an upper limit of agreement that 95% of the data should fall within.

The following parameters are used to create a Bland-Altman plot:

Bias = Average of the residuals (diff between observed and predicted HgB)

Standard Deviation (Std dev) of the residuals = 1.67

Lower Limits of Agreement = Std dev - 1.96 x Std Dev

Upper Limits of Agreement = Std dev + 1.96 x Std Dev

The Bland-Altman plot of the data points from Chip 1 and Chip 2 is shown as Figure 18.

This is a visual representation of how well the two methods of measurement (KUMC HgB

count and Chip HgB) agree with each other. The smaller range between the upper and lower limits of agreement, the better the agreement between the two methods.

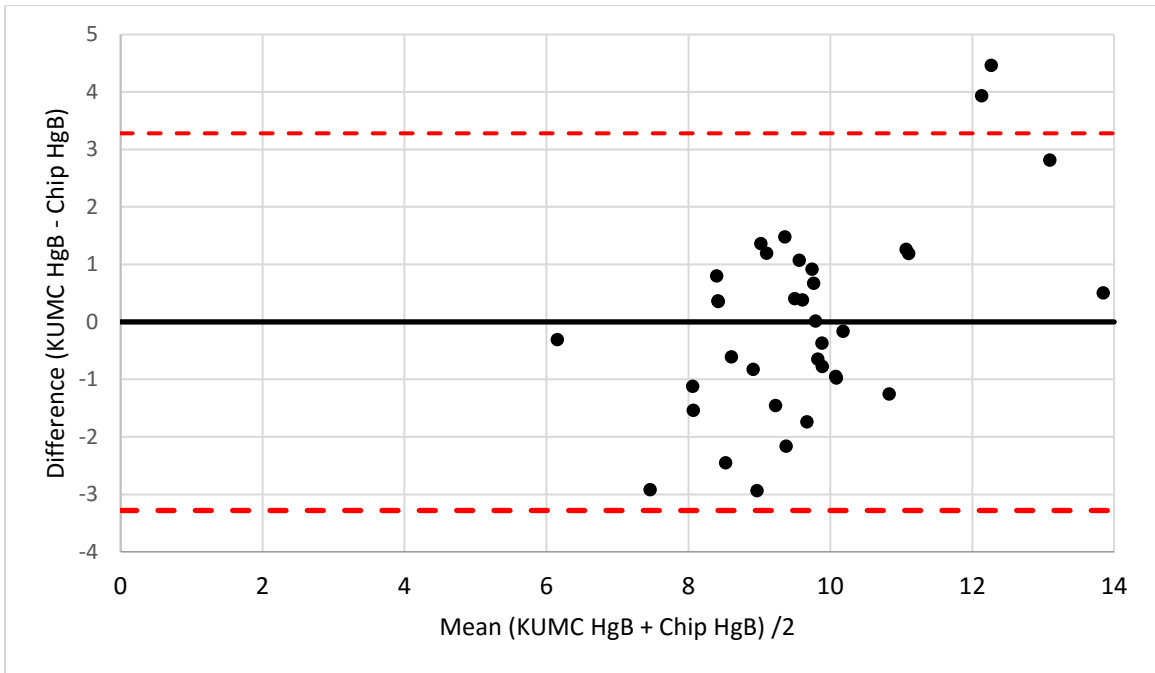


Figure 18. Bland-Altman plot showing visual correlation between known and predicted hemoglobin levels within 95% limits of agreement.

There have been many studies done to test the precision of POC hemoglobin monitoring devices [5-11] compared to hospital standards. Each study stresses the importance of accuracy whether a test should or should not be used depending on the outcome of the study. Out of 32 data points, all but two of the predicted hemoglobin levels are within one standard deviation (95% confidence interval or ± 3.2 limits of agreement). These statistics look good and meaningful but the clinical significance of the data must be considered [11]. In other words, does the 95% limits of agreement provide an acceptable level of accuracy for a diagnostic test to determining hemoglobin levels? With the range of hemoglobin levels being small between severe and healthy, an acceptable level of accuracy should be

less than 1g/dL because inaccurate readings in a clinical setting can have major health consequences. As shown in Figure 19, only 50% of the data are within +/- 1g/dL.

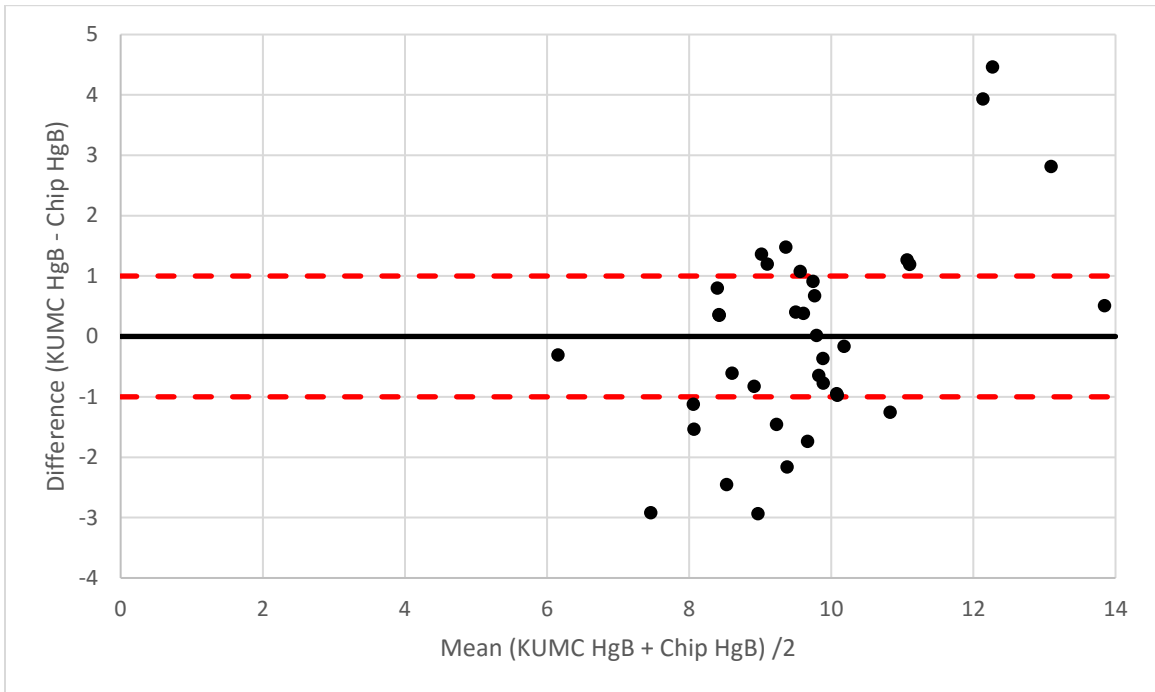


Figure 19. Bland-Altman plot showing visual correlation between known and predicted hemoglobin levels within +/-1 g/dL.

The observed vs. predicted hemoglobin levels were plotted using a column chart (see Figures 20 and 21) to visually represent the performance of the assay in both the chips and tubes. The charts show the same trends when estimating hemoglobin levels, so the assay performed the same in both. However, neither the chip nor the tube tests consistently predicted hemoglobin levels in the samples. Certain hemoglobin tests, such as the Pulse CO-Oximeter, have been shown to overestimate hemoglobin levels in lower values while underestimating them in higher values [12-13]. The same trend is evident in the chip and tube test data, with outliers on extreme ends of each data set. This indicates a possible missing element to the assay that can accurately detect high and low hemoglobin levels, and it is not necessarily an inconsistency based on error.

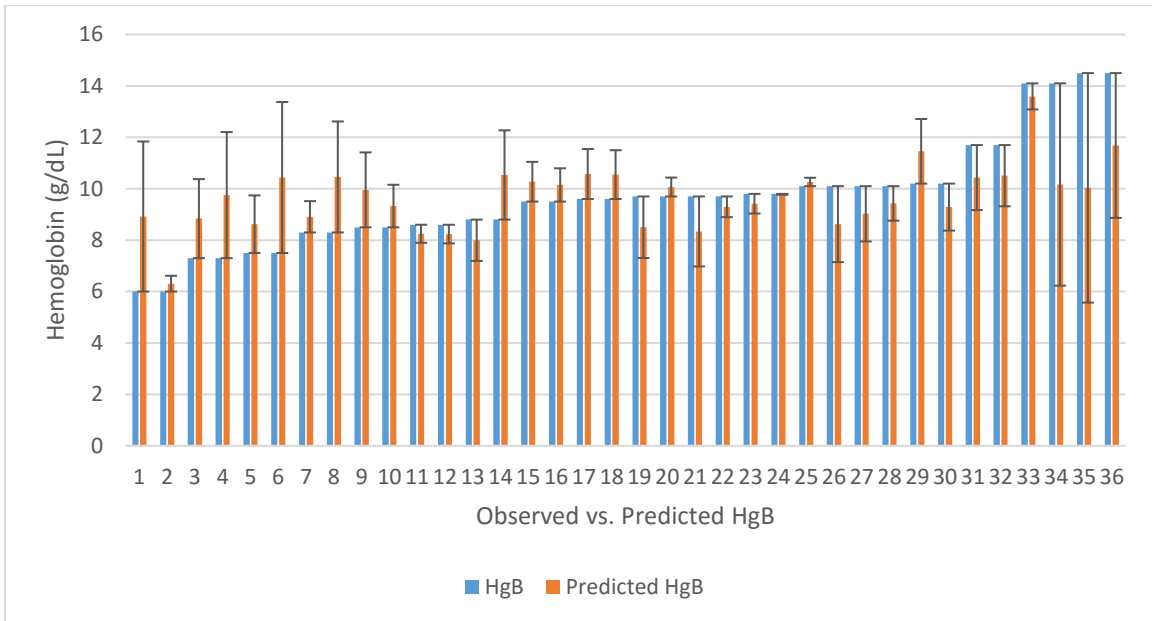


Figure 20. Column chart of known hemoglobin levels and predicted hemoglobin levels from Chip 1 and Chip 2.

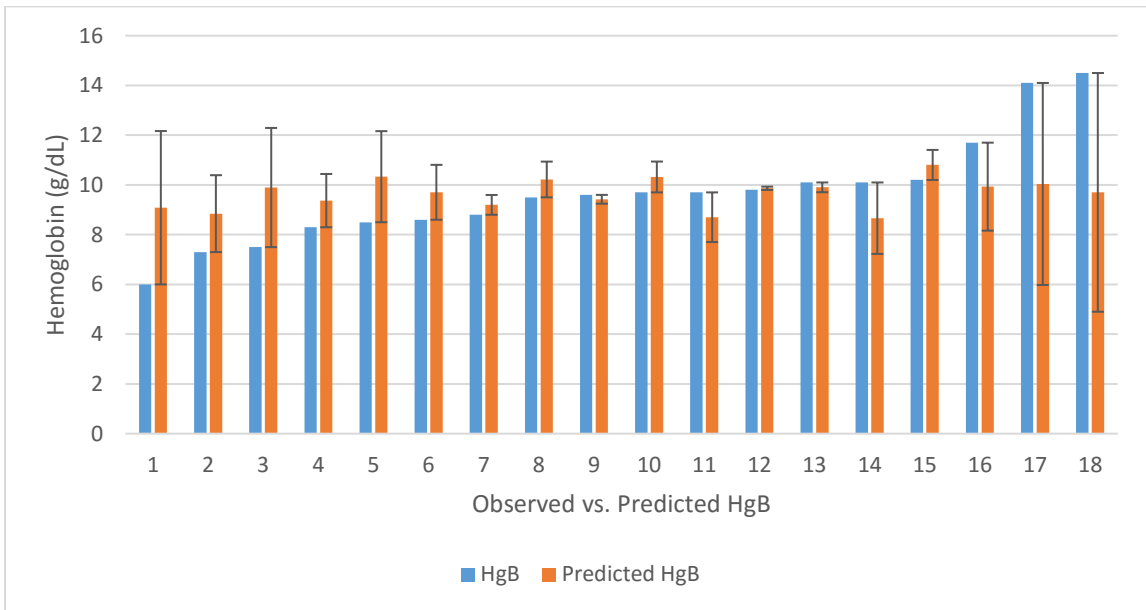


Figure 21. Column chart of known hemoglobin levels and predicted hemoglobin levels from Tubes.

References

1. Myles PS, Cui J. Using the Bland-Altman method to measure agreement with repeated measures. *Br J Anaesth.* 2007 SEP 2007;99(3):309-11.
2. Bland JM, Altman DG. Agreement between methods of measurement with multiple observations per individual. *J Biopharm Stat* 2007; 17: 571–82
3. Myles PS, Cui J. Using the Bland-Altman method to measure agreement with repeated measures. *Br J Anaesth.* 2007 SEP 2007;99(3):309-11.
4. Bland JM, Altman DG. Statistical methods for assessing agreement between two methods of clinical measurement. *Lancet* 1986; i: 307–10
5. Gayat E, Bodin A, Sportiello C, et al. Performance evaluation of a noninvasive hemoglobin monitoring device. *Ann Emerg Med* 2011; 57: 330–3
6. Gayat E, Aulagnier J, Matthieu E, Boisson M, Fischler M. Non-invasive measurement of haemoglobin: assessment of two different point-of-care technologies. *PLoS ONE* 2012; 7: e30065
7. Frasca D, Dahyot-Fizelier C, Catherine K, Levrat Q, Debaene B, Mimoz O. Accuracy of a continuous noninvasive hemoglobin monitor in intensive care unit patients. *Crit Care Med* 2011; 39: 2277–82
8. Coquin J, Dewitte A, Manach YL, et al. Precision of noninvasive hemoglobin-level measurement by pulse co-oximetry in patients admitted to intensive care units for severe gastrointestinal bleeds. *Crit Care Med* 2012; 40: 2576–82
9. Causey MW, Miller S, Foster A, Beekley A, Zenger D, Martin M. Validation of noninvasive hemoglobin measurements using the Masimo Radical-7 SpHb Station. *Am J Surg* 2011; 201: 592–8

10. Seguin P, Kleiber A, Chanavaz C, Morcet J, Malledant Y. Determination of capillary hemoglobin levels using the HemoCue system in intensive care patients. *J Crit Care.* 2011 AUG 2011;26(4):423-7.
11. Nguyen B-V, Vincent J-L, Nowak E, et al. The accuracy of noninvasive hemoglobin measurement by multiwavelength pulse oximetry after cardiac surgery. *Anesth Analg* 2011; 113: 1052–7
12. Rice MJ, Gravenstein N, Morey TE. Noninvasive Hemoglobin Monitoring: How Accurate Is Enough? *Anesth Analg.* 2013 OCT 2013;117(4):902-7.
13. Giraud B, Frasca D, Debaene B, Mimoz O. Comparison of haemoglobin measurement methods in the operating theatre. *Br J Anaesth.* 2013 DEC 2013;111(6):946-54.

Chapter 7 - Conclusions





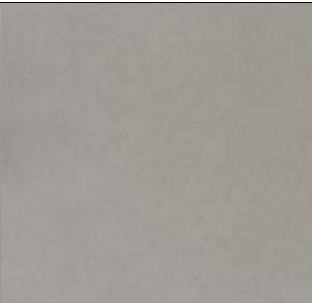

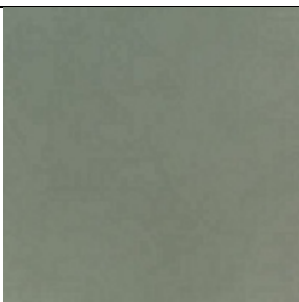

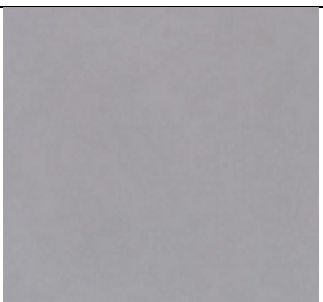
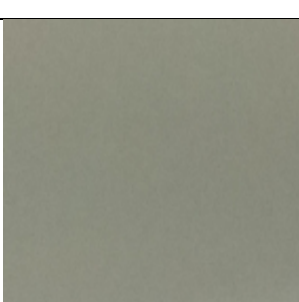
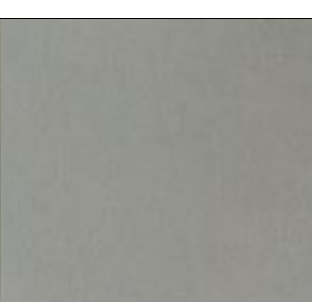

The objective of this study was twofold: 1) design and fabricate a 3D printed, low cost microfluidic mixing chip and 2) develop an anemia diagnostic assay for detecting anemia using the mixing chip. Combined, the mixing chip and assay would act as a proof of concept for the microfluidic chip working as a diagnostic device.



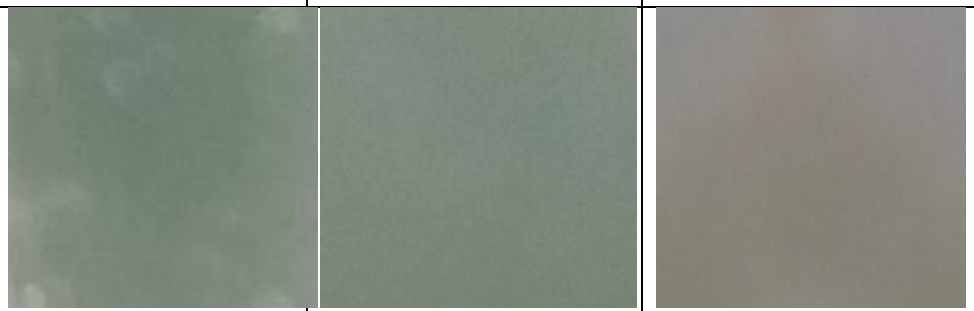
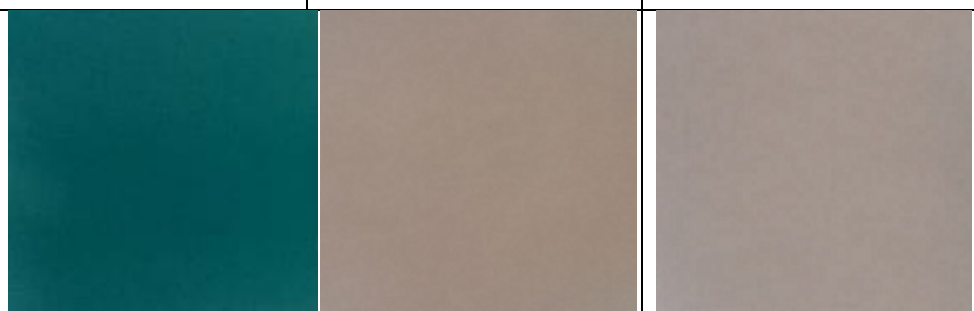
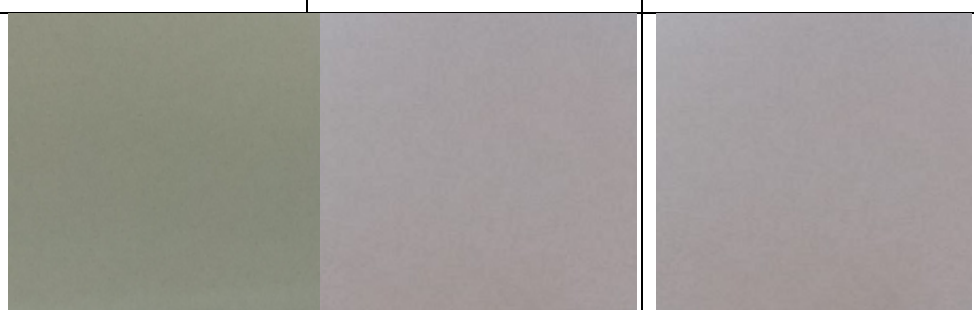
Hemoglobin powder in a buffer solution and TMB/H₂O₂ were introduced within the chips to test the mixing efficiency. Chip A (initial design) did not show a uniform color change throughout the chip indicating incomplete mixing. Chip B, optimized using a 3D computational fluid dynamic simulation model, showed uniform color change throughout. During clinical validation, RGB values of the color change within the chip window showed consistent and repeatable results. Column charts of the ImageJ RGB values in replicate tests for each sample (Chip 1 and Chip 2) showed consistent and repeatable results. This indicated that the Chip B design works well as a mixing chip.

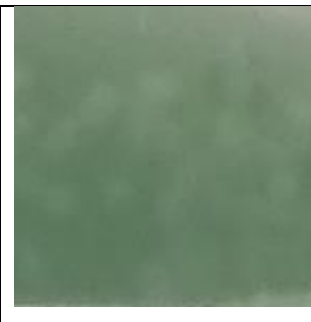

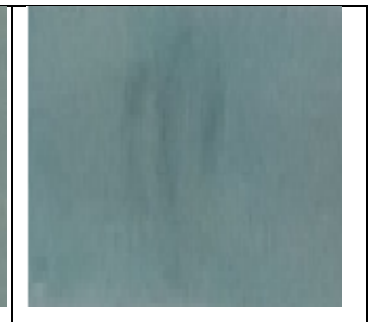

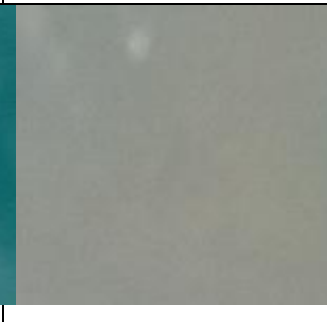
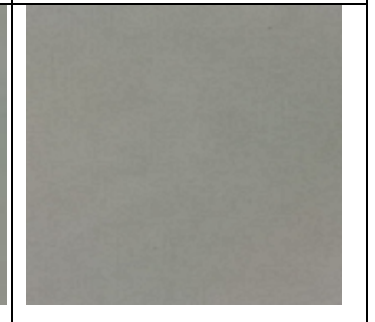
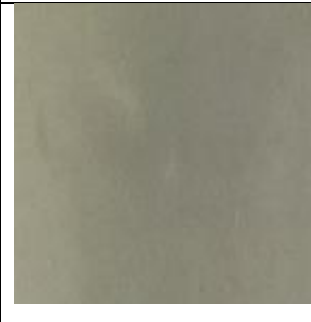
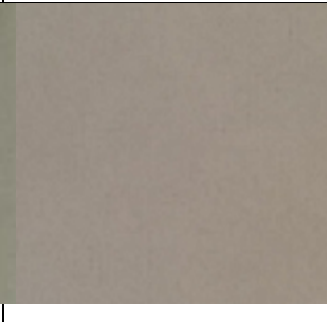
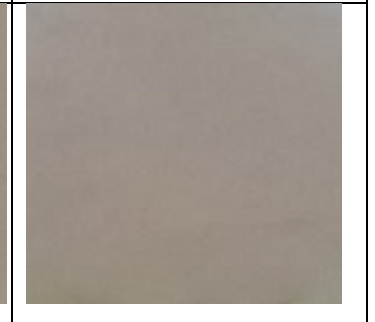
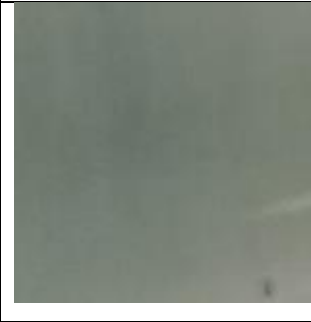




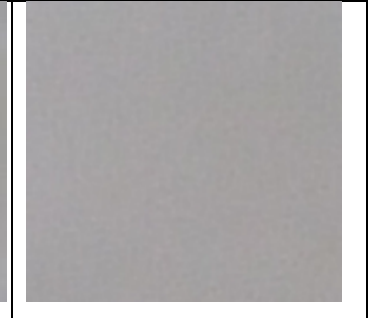
Neither the chip nor the tube tests consistently predicted hemoglobin levels in the samples. They tended to overestimate hemoglobin levels in lower values while underestimating them in higher values. The over and under estimating of hemoglobin levels could be due to the small data set (18 patient samples). Out of 18 samples, only two were within a healthy range while three were within the severe range. A larger number of samples with a distribution across the full range of hemoglobin values (from severe to normal) would improve the accuracy of the regression analysis.





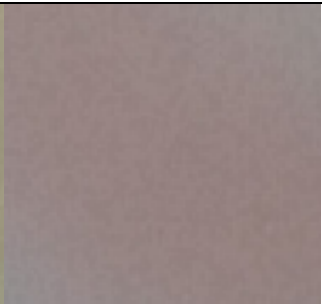
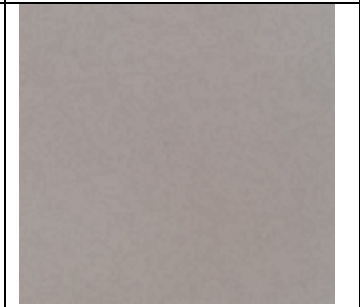
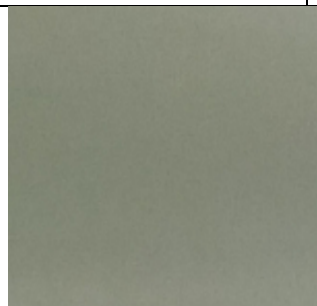
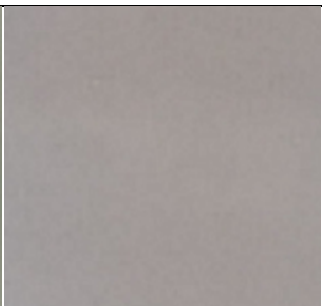
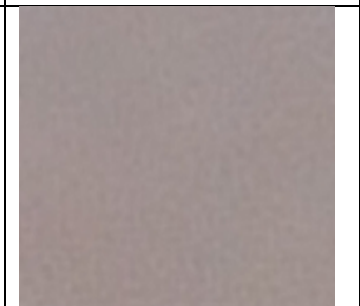
The clinical samples collected for this study were preserved with acid citrate dextrose (ACD). While the color change reaction between TMB and hemoglobin has been demonstrated in this study, the possible effect of the ACD on the TMB oxidation reaction and predicted hemoglobin levels was not evaluated. Future studies should test blood samples without preservatives to ascertain whether ACD effects the performance of the assay. Since blood without preservatives would be used in a POC setting, this is a logical next step.

Appendix A - Digital Images of Assay Color Change Reactions

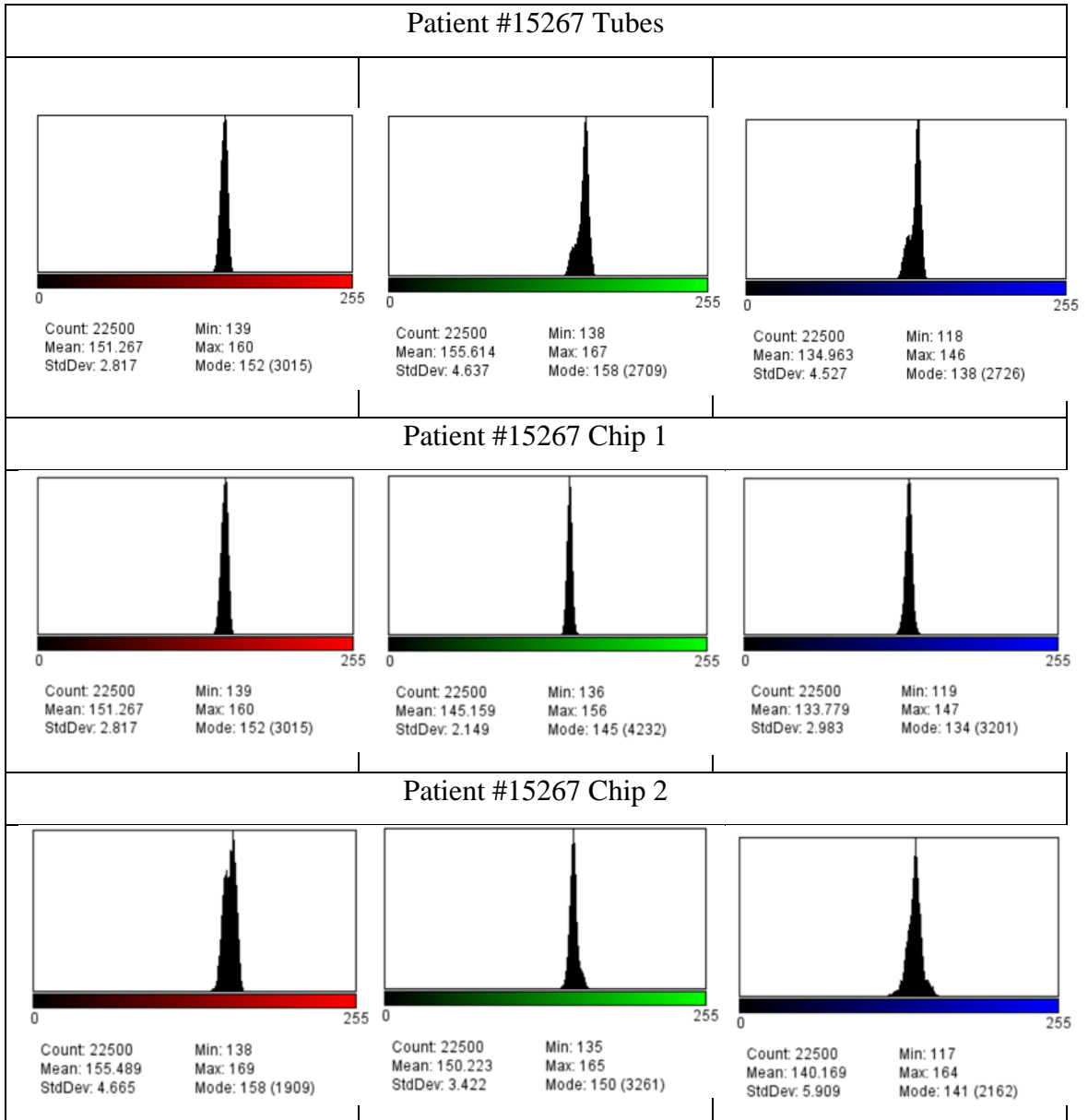
Patient	Hgb	Tube	Chip 1	Chip 2
15267	6			
17669	7.3			
017193	7.5			
12218	8.3			

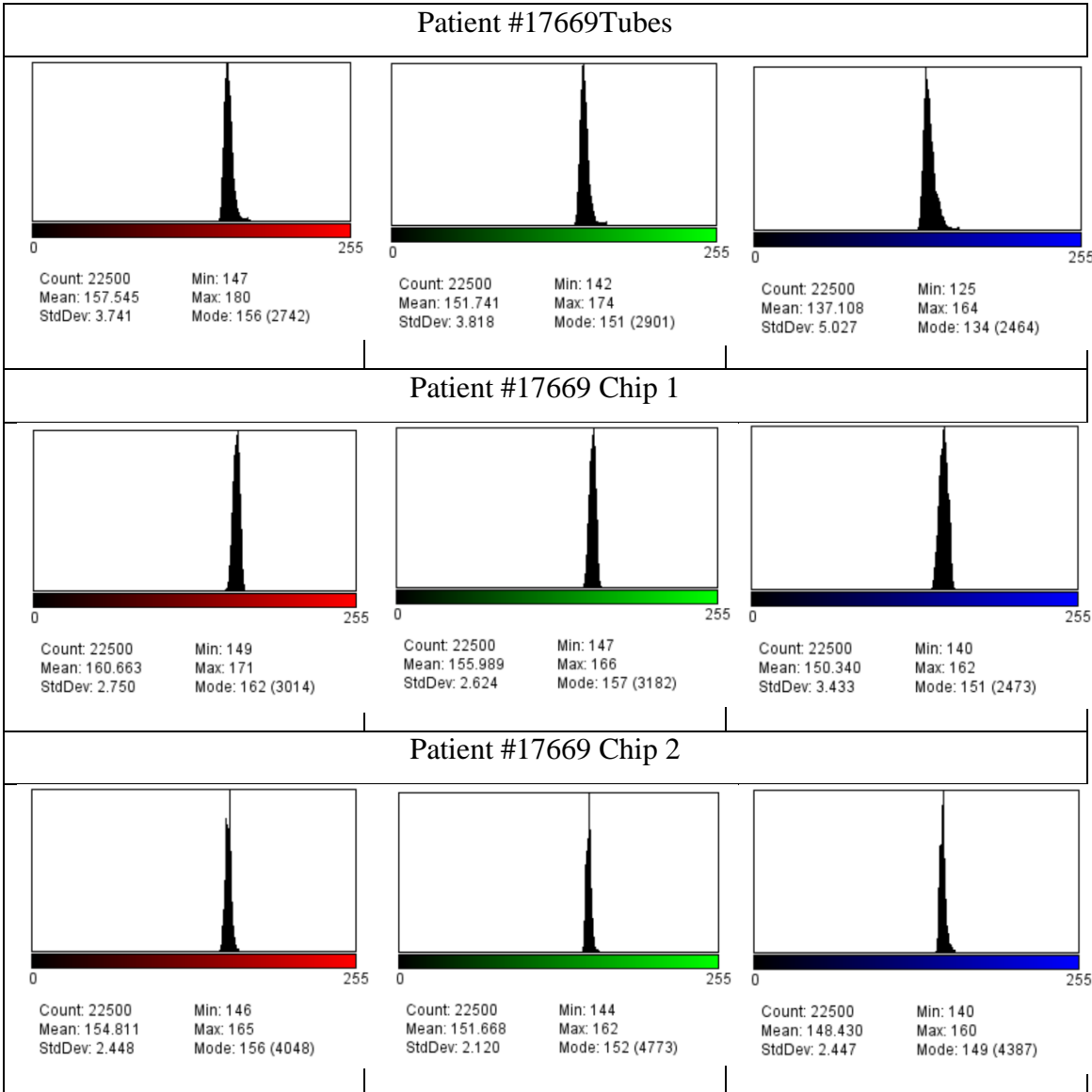
16367	8.5	
020258	8.6	
020452	8.8	
005996	9.5	
20737	9.6	

019262	9.7			
005675	9.7			
003659	9.8			
020485	10.1			
15429	10.1			

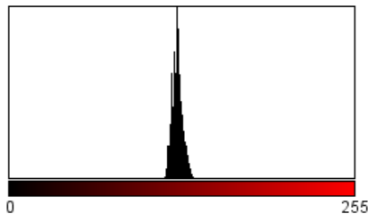
014476	10.2			
20247	11.7			
16701	14.1			

Appendix B - ImageJ RGB Histograms

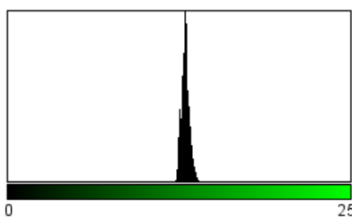




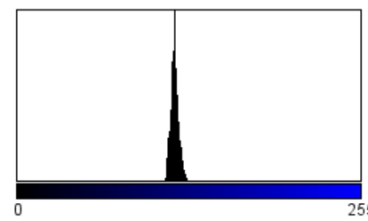
Patient #17193 Tubes



Count: 22500
Mean: 124.197
StdDev: 3.841
Min: 114
Max: 138
Mode: 124 (3014)

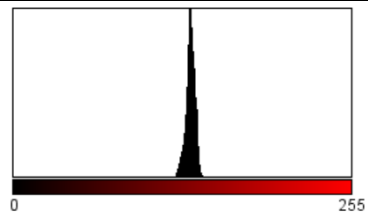


Count: 22500
Mean: 132.221
StdDev: 3.024
Min: 124
Max: 144
Mode: 132 (3577)

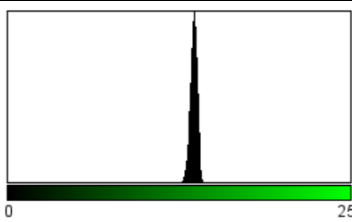


Count: 22500
Mean: 116.941
StdDev: 2.989
Min: 109
Max: 128
Mode: 117 (3876)

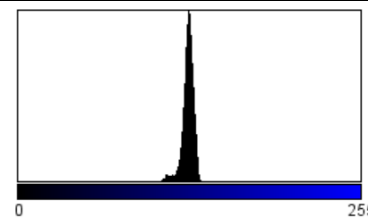
Patient #17193 Chip 1



Count: 22500
Mean: 133.802
StdDev: 3.526
Min: 121
Max: 148
Mode: 133 (2797)

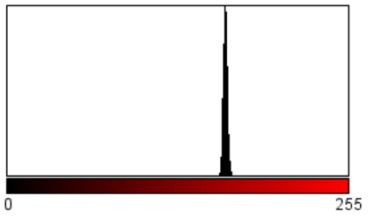


Count: 22500
Mean: 138.536
StdDev: 2.680
Min: 128
Max: 150
Mode: 139 (3321)

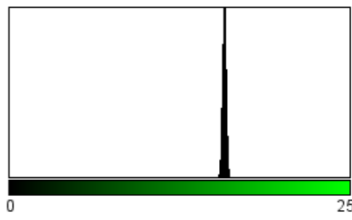


Count: 22500
Mean: 126.547
StdDev: 4.484
Min: 104
Max: 140
Mode: 127 (2550)

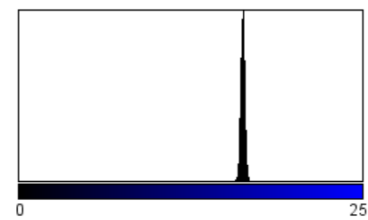
Patient #17193 Chip 2



Count: 22500
Mean: 163.316
StdDev: 1.633
Min: 156
Max: 169
Mode: 163 (5165)

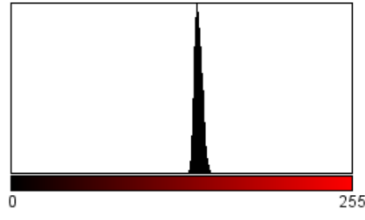


Count: 22500
Mean: 161.297
StdDev: 1.539
Min: 156
Max: 167
Mode: 162 (5290)

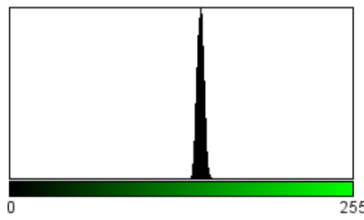


Count: 22500
Mean: 166.445
StdDev: 1.658
Min: 160
Max: 173
Mode: 167 (5206)

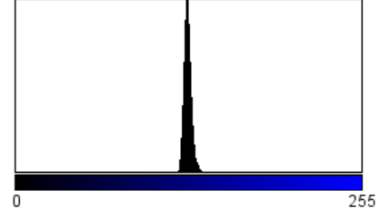
Patient #12218 Tubes



Count: 22500 Min: 131
Mean: 140.145 Max: 151
StdDev: 2.969 Mode: 139 (2925)

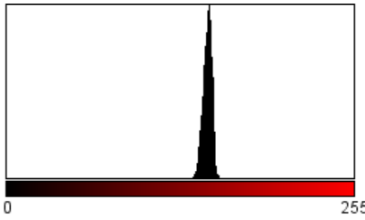


Count: 22500 Min: 132
Mean: 141.864 Max: 153
StdDev: 2.662 Mode: 142 (3148)

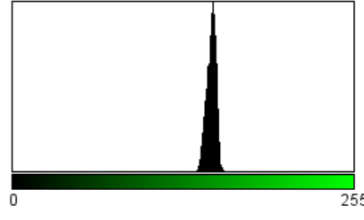


Count: 22500 Min: 118
Mean: 126.867 Max: 139
StdDev: 2.773 Mode: 126 (3328)

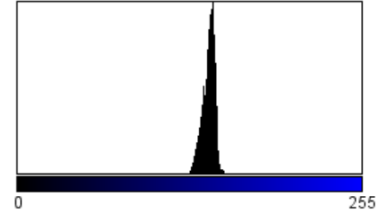
Patient #12218 Chip 1



Count: 22500 Min: 135
Mean: 147.631 Max: 157
StdDev: 3.314 Mode: 149 (2720)

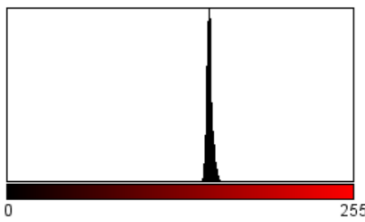


Count: 22500 Min: 137
Mean: 148.701 Max: 159
StdDev: 3.603 Mode: 150 (2579)

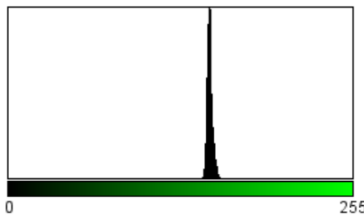


Count: 22500 Min: 126
Mean: 141.806 Max: 156
StdDev: 4.530 Mode: 145 (2283)

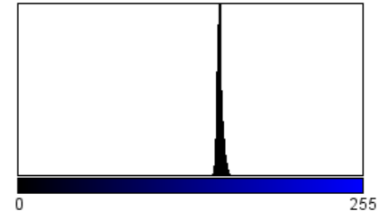
Patient #12218 Chip 2



Count: 22500 Min: 124
Mean: 149.362 Max: 199
StdDev: 3.132 Mode: 149 (4361)

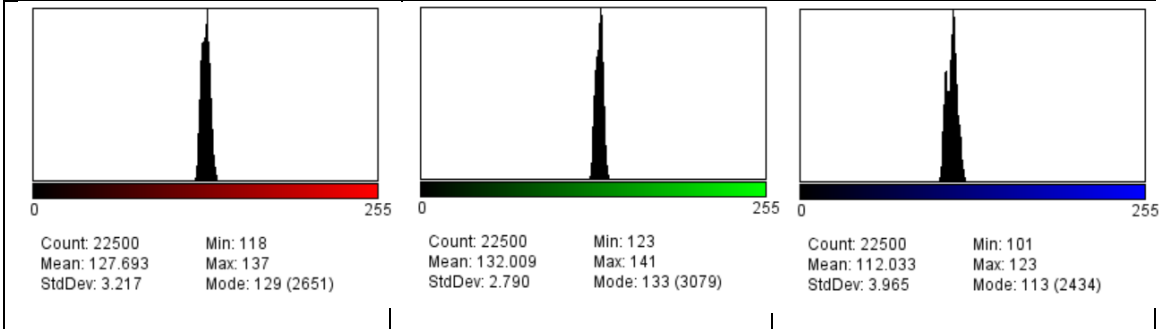


Count: 22500 Min: 124
Mean: 149.509 Max: 199
StdDev: 3.068 Mode: 149 (4479)

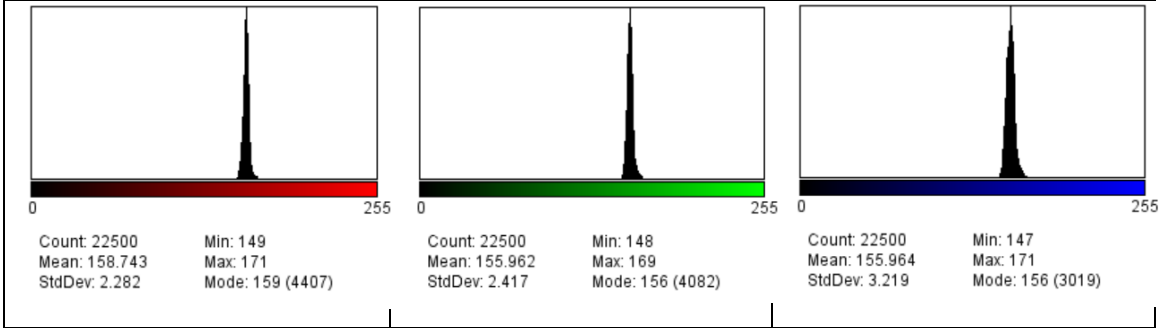


Count: 22500 Min: 124
Mean: 149.530 Max: 199
StdDev: 3.079 Mode: 150 (4448)

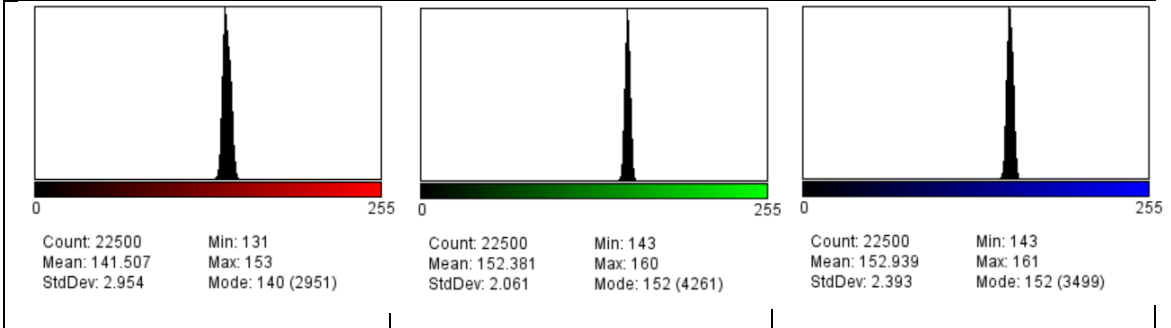
Patient #16367 Tubes



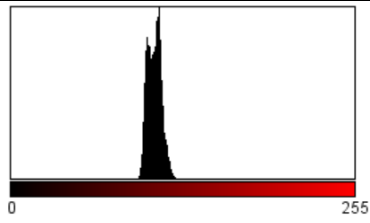
Patient #16367 Chip 1



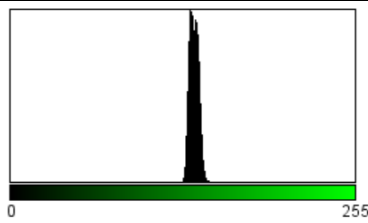
Patient #16367 Chip 2



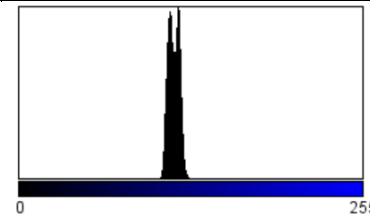
Patient #20258 Tubes



Count: 22500 Min: 92
Mean: 106.440 Max: 125
StdDev: 5.135 Mode: 110 (1743)

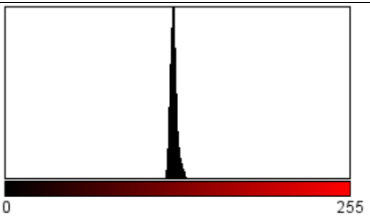


Count: 22500 Min: 124
Mean: 135.975 Max: 153
StdDev: 3.450 Mode: 133 (2252)

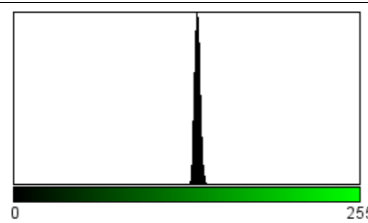


Count: 22500 Min: 100
Mean: 114.855 Max: 131
StdDev: 4.117 Mode: 118 (1930)

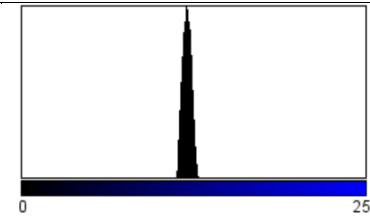
Patient #20258 Chip 1



Count: 22500 Min: 116
Mean: 124.617 Max: 137
StdDev: 2.639 Mode: 125 (3616)

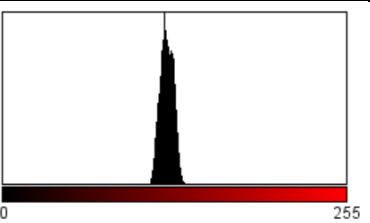


Count: 22500 Min: 128
Mean: 135.408 Max: 148
StdDev: 2.155 Mode: 135 (3868)

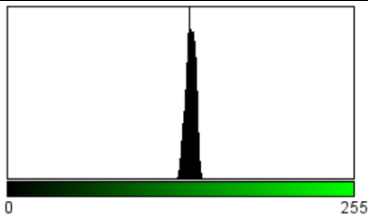


Count: 22500 Min: 113
Mean: 122.460 Max: 134
StdDev: 3.323 Mode: 122 (2423)

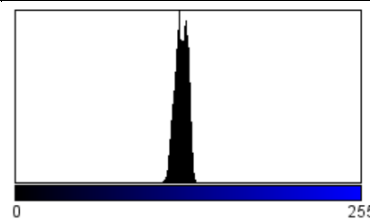
Patient #20258 Chip 2



Count: 22500 Min: 108
Mean: 121.787 Max: 136
StdDev: 4.895 Mode: 120 (1816)

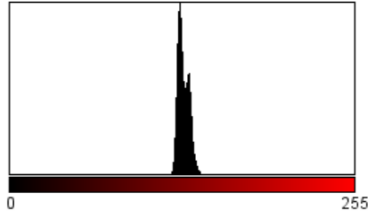


Count: 22500 Min: 122
Mean: 134.904 Max: 144
StdDev: 3.589 Mode: 134 (2446)

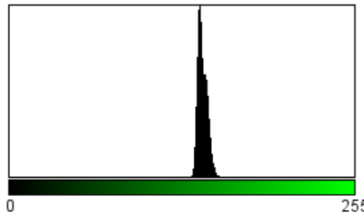


Count: 22500 Min: 107
Mean: 122.529 Max: 135
StdDev: 4.610 Mode: 121 (1815)

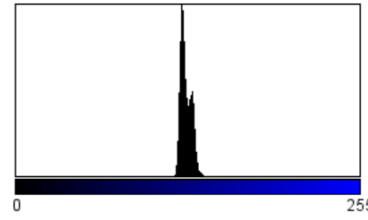
Patient #20452 Tubes



Count: 22500
Mean: 128.733
StdDev: 4.539
Min: 118
Max: 160
Mode: 126 (2435)

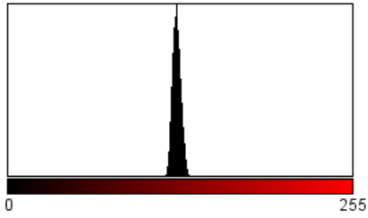


Count: 22500
Mean: 143.034
StdDev: 3.975
Min: 132
Max: 174
Mode: 141 (2773)

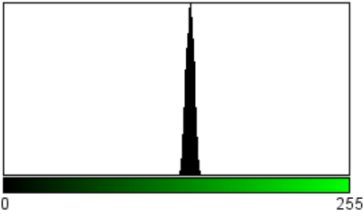


Count: 22500
Mean: 126.299
StdDev: 4.394
Min: 115
Max: 157
Mode: 123 (2736)

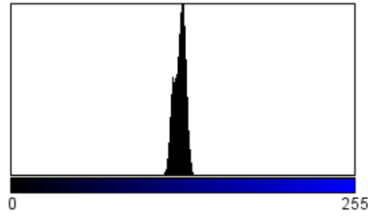
Patient #20452 Chip 1



Count: 22500
Mean: 124.954
StdDev: 3.132
Min: 114
Max: 138
Mode: 125 (2892)

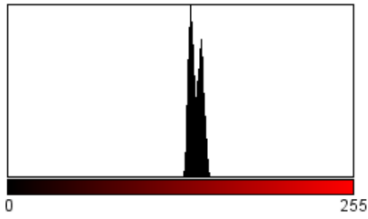


Count: 22500
Mean: 137.534
StdDev: 2.983
Min: 127
Max: 149
Mode: 138 (2809)

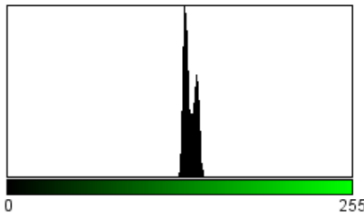


Count: 22500
Mean: 125.246
StdDev: 4.198
Min: 111
Max: 139
Mode: 127 (2160)

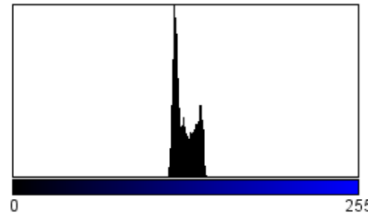
Patient #20452 Chip 2



Count: 22500
Mean: 138.761
StdDev: 4.437
Min: 129
Max: 151
Mode: 135 (2141)

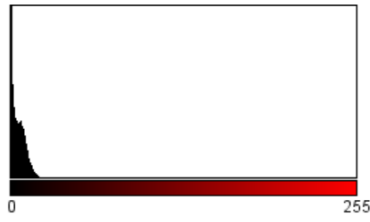


Count: 22500
Mean: 135.087
StdDev: 4.383
Min: 127
Max: 148
Mode: 131 (2544)

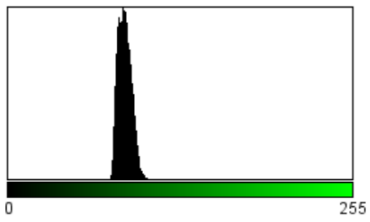


Count: 22500
Mean: 126.614
StdDev: 7.808
Min: 114
Max: 144
Mode: 119 (2138)

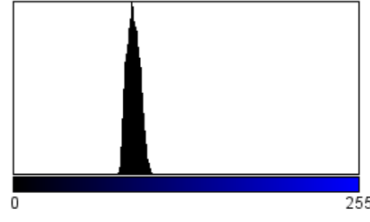
Patient #5996 Tubes



Count: 22500
Mean: 5.279
StdDev: 4.681
Min: 0
Max: 28
Mode: 0 (4316)

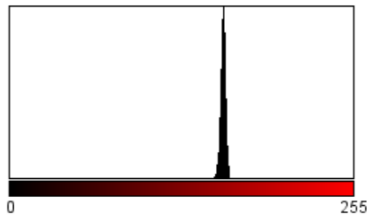


Count: 22500
Mean: 86.312
StdDev: 4.981
Min: 74
Max: 108
Mode: 85 (1642)

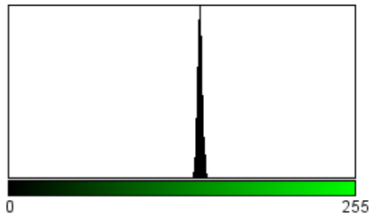


Count: 22500
Mean: 88.304
StdDev: 4.853
Min: 75
Max: 107
Mode: 87 (1738)

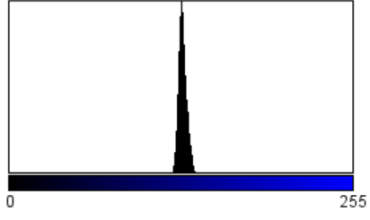
Patient #5996 Chip 1



Count: 22500
Mean: 158.618
StdDev: 1.924
Min: 150
Max: 165
Mode: 159 (4722)

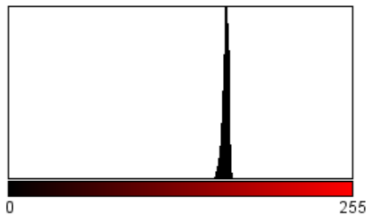


Count: 22500
Mean: 140.855
StdDev: 1.901
Min: 135
Max: 148
Mode: 141 (4709)

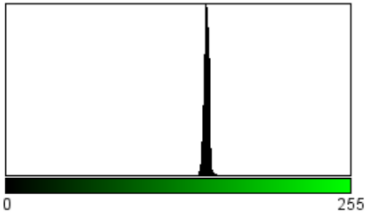


Count: 22500
Mean: 128.835
StdDev: 3.001
Min: 120
Max: 140
Mode: 128 (3194)

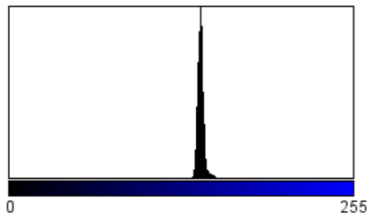
Patient #5996 Chip 2



Count: 22500
Mean: 161.181
StdDev: 2.364
Min: 151
Max: 168
Mode: 161 (3827)

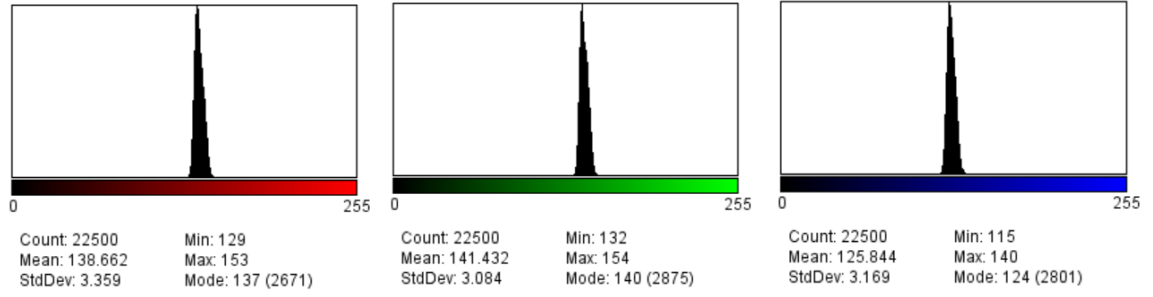


Count: 22500
Mean: 148.664
StdDev: 2.012
Min: 140
Max: 160
Mode: 148 (4332)

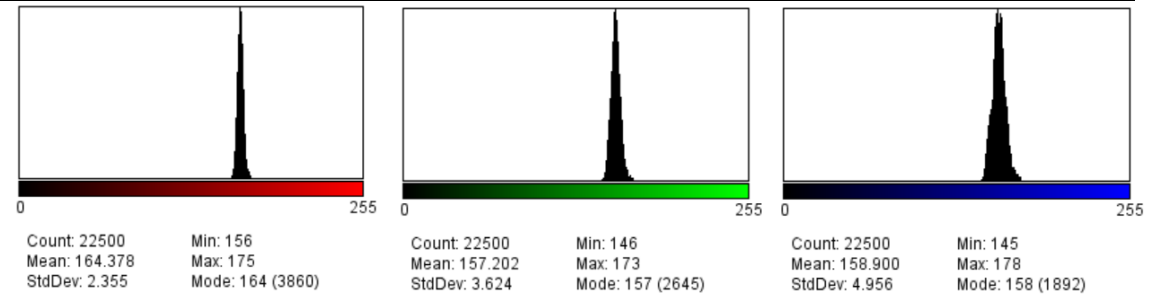


Count: 22500
Mean: 142.081
StdDev: 2.493
Min: 134
Max: 158
Mode: 142 (4325)

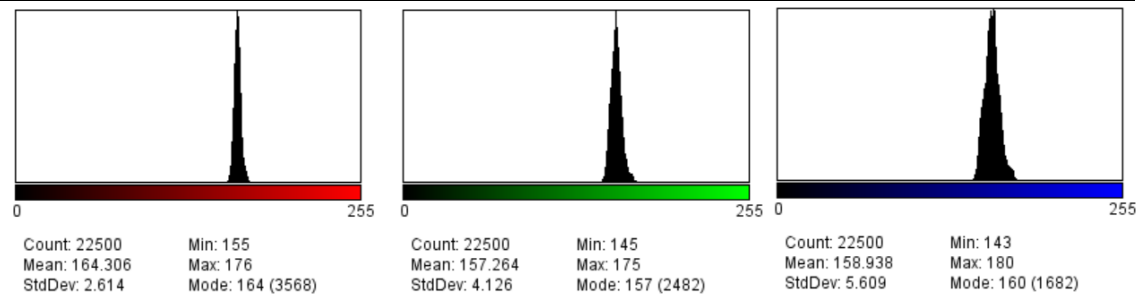
Patient #20737 Tubes



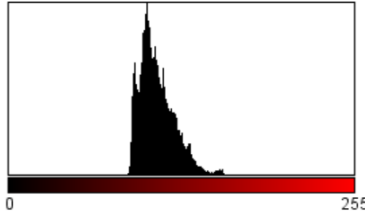
Patient #20737 Chip 1



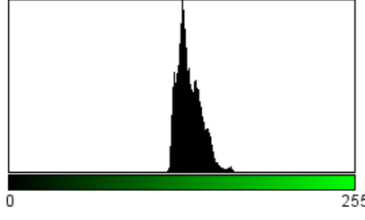
Patient #20737 Chip 2



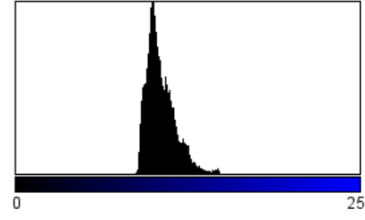
Patient #19262 Tubes



Count: 22500
Mean: 109.359
StdDev: 13.002
Min: 84
Max: 162
Mode: 102 (961)

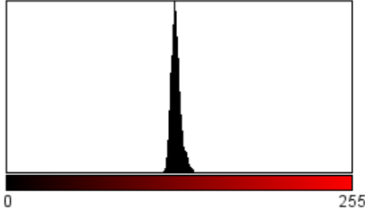


Count: 22500
Mean: 133.157
StdDev: 8.958
Min: 113
Max: 168
Mode: 128 (1363)

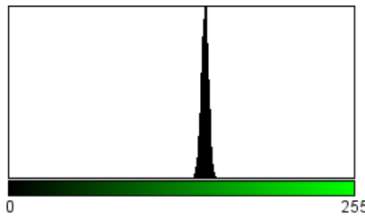


Count: 22500
Mean: 107.619
StdDev: 10.990
Min: 85
Max: 154
Mode: 101 (1159)

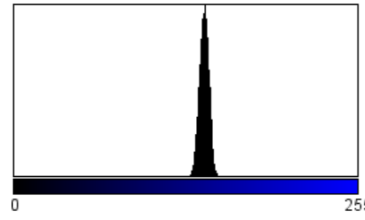
Patient #19262 Chip 1



Count: 22500
Mean: 125.029
StdDev: 3.677
Min: 114
Max: 140
Mode: 124 (2847)

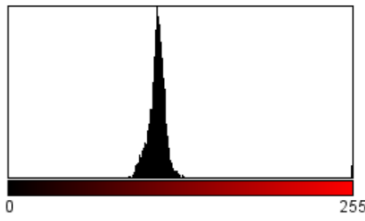


Count: 22500
Mean: 144.854
StdDev: 2.830
Min: 133
Max: 155
Mode: 146 (3087)

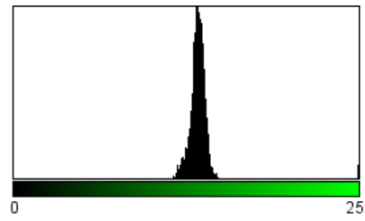


Count: 22500
Mean: 141.295
StdDev: 3.553
Min: 126
Max: 153
Mode: 142 (2449)

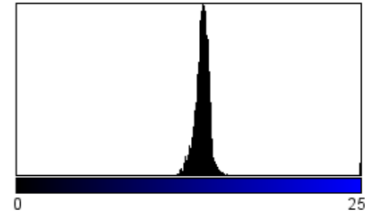
Patient #19262 Chip 2



Count: 22500
Mean: 110.862
StdDev: 13.283
Min: 87
Max: 255
Mode: 110 (1943)

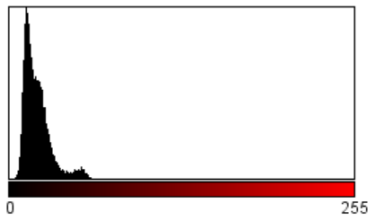


Count: 22500
Mean: 136.774
StdDev: 11.040
Min: 113
Max: 255
Mode: 135 (1895)

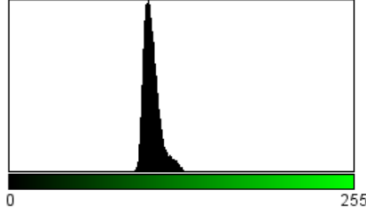


Count: 22500
Mean: 138.295
StdDev: 10.893
Min: 114
Max: 255
Mode: 138 (1940)

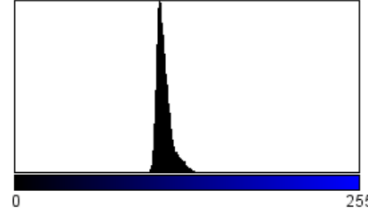
Patient #5675 Tubes



Count: 22500
Mean: 20.154
StdDev: 10.259
Min: 1
Max: 69
Mode: 12 (1471)

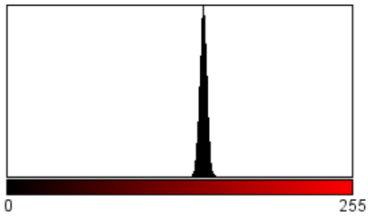


Count: 22500
Mean: 105.503
StdDev: 6.246
Min: 89
Max: 138
Mode: 103 (1739)

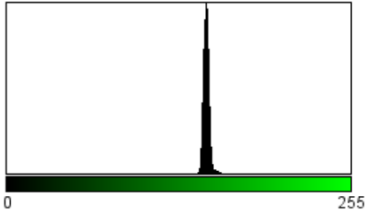


Count: 22500
Mean: 110.278
StdDev: 5.557
Min: 96
Max: 143
Mode: 107 (2176)

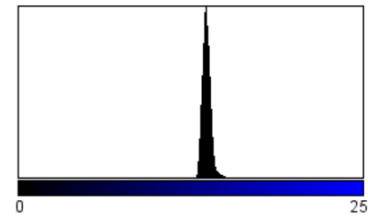
Patient #5675 Chip 1



Count: 22500
Mean: 145.120
StdDev: 2.950
Min: 134
Max: 169
Mode: 145 (3273)

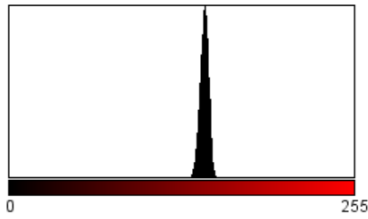


Count: 22500
Mean: 148.231
StdDev: 2.563
Min: 139
Max: 174
Mode: 148 (3952)

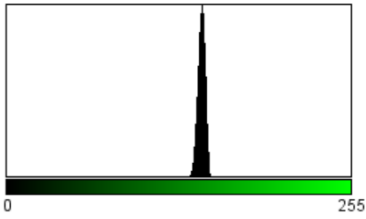


Count: 22500
Mean: 139.350
StdDev: 3.422
Min: 129
Max: 168
Mode: 139 (3033)

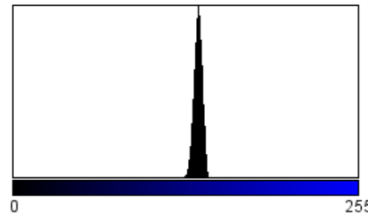
Patient #5675 Chip 2



Count: 22500
Mean: 144.399
StdDev: 3.220
Min: 125
Max: 154
Mode: 145 (2737)

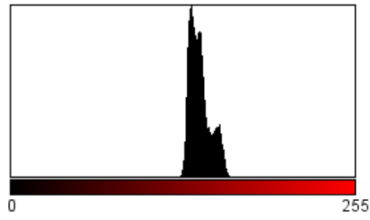


Count: 22500
Mean: 144.495
StdDev: 2.772
Min: 125
Max: 153
Mode: 145 (3079)

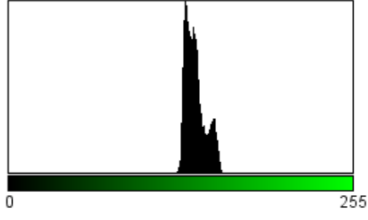


Count: 22500
Mean: 136.794
StdDev: 3.097
Min: 117
Max: 145
Mode: 137 (2893)

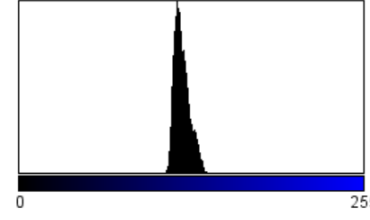
Patient #3659 Tubes



Count: 22500
Mean: 140.131
StdDev: 7.728
Min: 124
Max: 164
Mode: 134 (1396)

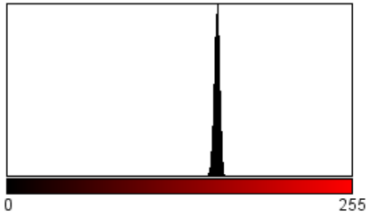


Count: 22500
Mean: 138.331
StdDev: 7.466
Min: 121
Max: 161
Mode: 131 (1504)

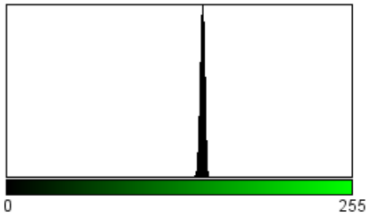


Count: 22500
Mean: 120.595
StdDev: 5.754
Min: 104
Max: 142
Mode: 117 (1772)

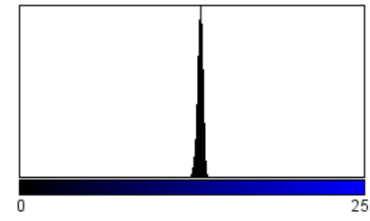
Patient #3659 Chip 1



Count: 22500
Mean: 155.358
StdDev: 2.131
Min: 147
Max: 163
Mode: 156 (4115)

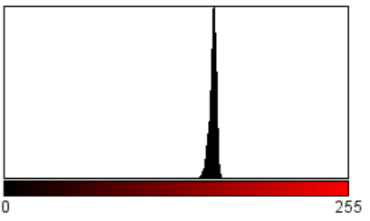


Count: 22500
Mean: 144.732
StdDev: 1.809
Min: 136
Max: 151
Mode: 145 (4598)

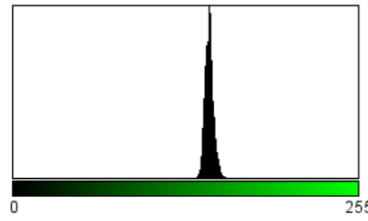


Count: 22500
Mean: 133.623
StdDev: 2.157
Min: 125
Max: 142
Mode: 134 (4141)

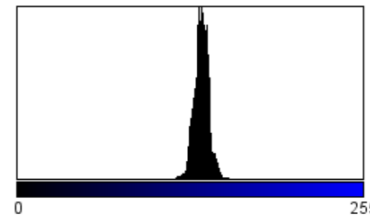
Patient #3659 Chip 2



Count: 22500
Mean: 154.942
StdDev: 2.770
Min: 139
Max: 163
Mode: 156 (3645)

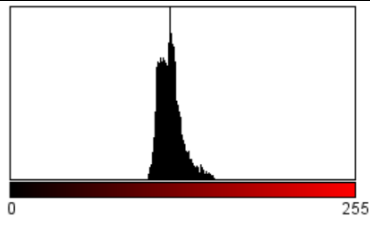


Count: 22500
Mean: 145.025
StdDev: 3.284
Min: 132
Max: 162
Mode: 145 (3087)

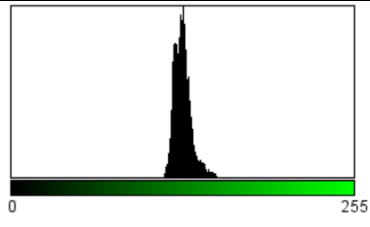


Count: 22500
Mean: 135.948
StdDev: 5.530
Min: 115
Max: 162
Mode: 134 (1721)

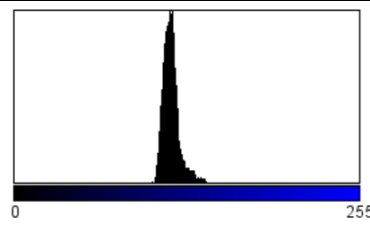
Patient #20485 Tubes



Count: 22500
Mean: 118.438
StdDev: 8.760
Min: 101
Max: 157
Mode: 118 (1404)

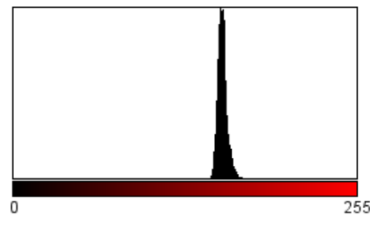


Count: 22500
Mean: 127.527
StdDev: 6.510
Min: 110
Max: 163
Mode: 128 (1652)

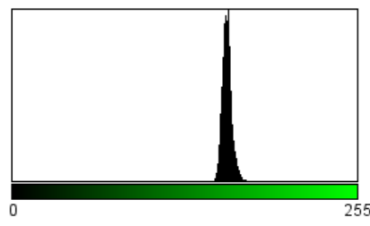


Count: 22500
Mean: 115.889
StdDev: 6.247
Min: 99
Max: 151
Mode: 117 (1720)

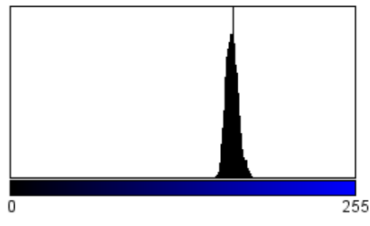
Patient #20485 Chip 1



Count: 22500
Mean: 155.443
StdDev: 3.588
Min: 144
Max: 172
Mode: 154 (2682)

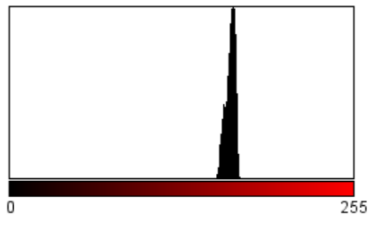


Count: 22500
Mean: 158.936
StdDev: 3.596
Min: 146
Max: 175
Mode: 160 (2694)

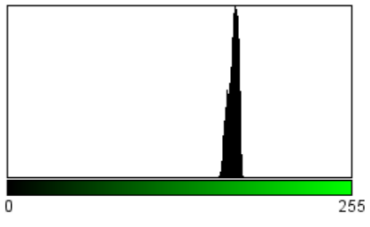


Count: 22500
Mean: 164.194
StdDev: 4.591
Min: 150
Max: 180
Mode: 165 (2167)

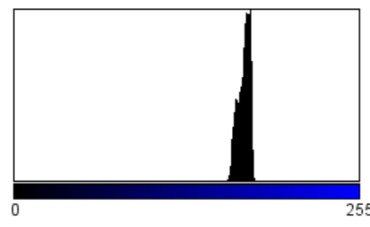
Patient #20485 Chip 2



Count: 22500
Mean: 163.906
StdDev: 3.630
Min: 151
Max: 172
Mode: 166 (2521)

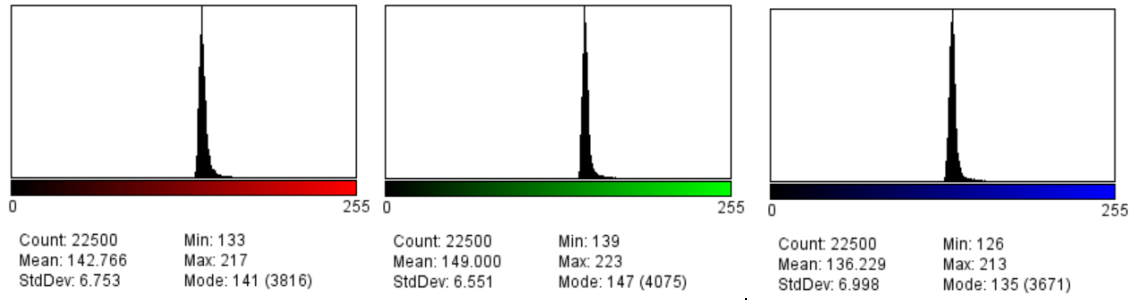


Count: 22500
Mean: 167.585
StdDev: 3.728
Min: 155
Max: 175
Mode: 169 (2368)

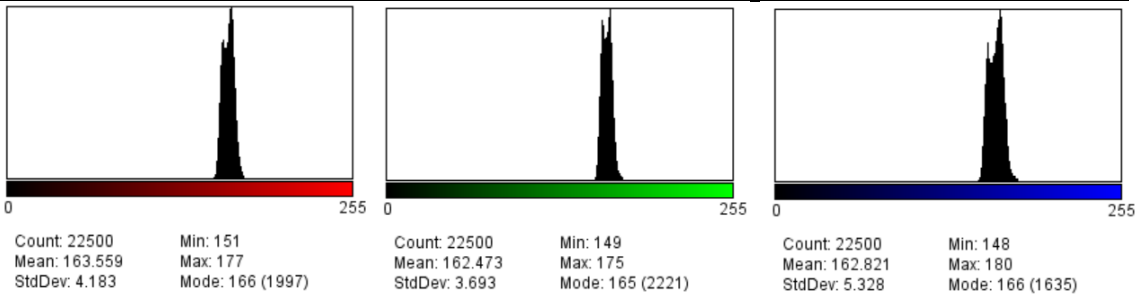


Count: 22500
Mean: 170.094
StdDev: 4.408
Min: 156
Max: 179
Mode: 175 (2102)

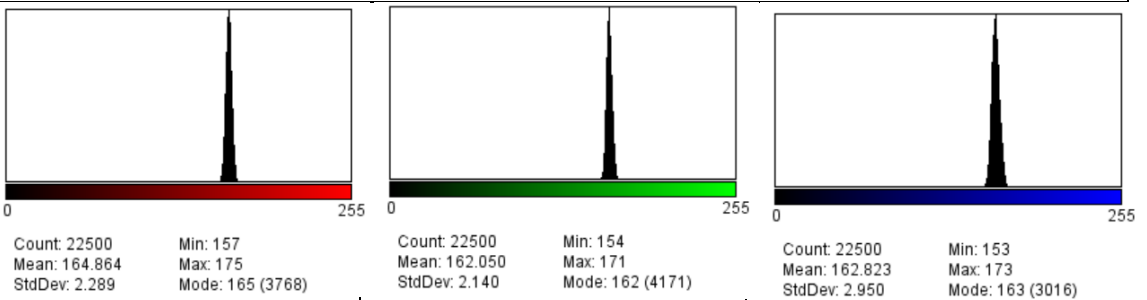
Patient #15429 Tubes



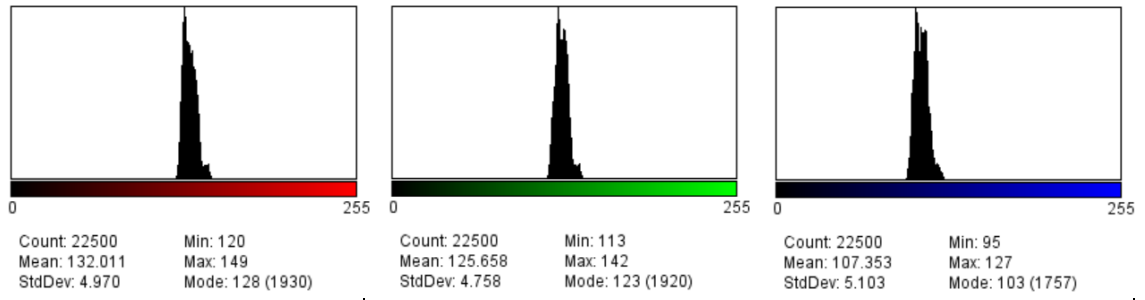
Patient #15429 Chip 1



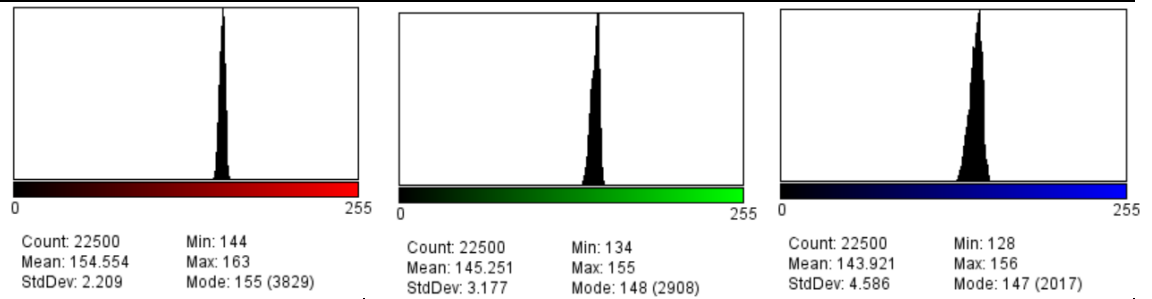
Patient #15429 Chip 2



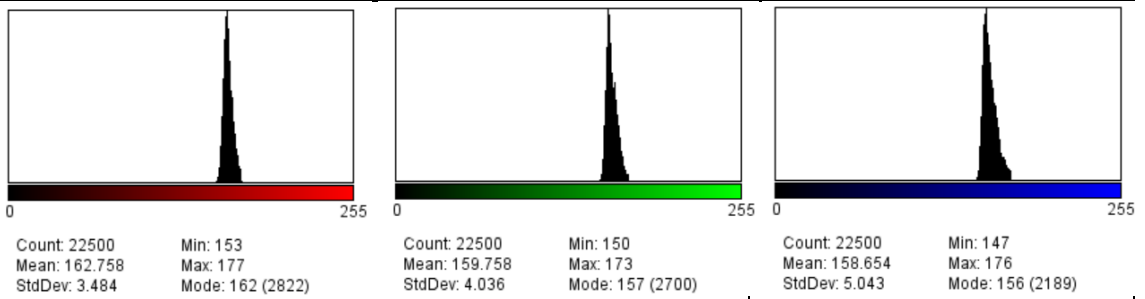
Patient #14476 Tubes



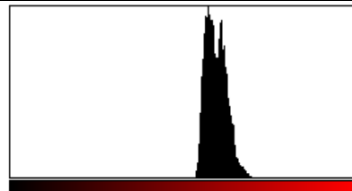
Patient #14476 Chip 1



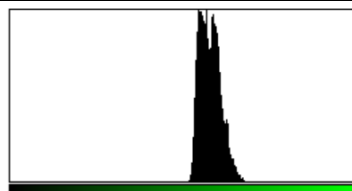
Patient #14476 Chip 2



Patient #20247 Tubes



Count: 22500
Mean: 152.937
StdDev: 7.718
Min: 135
Max: 185
Mode: 147 (1145)

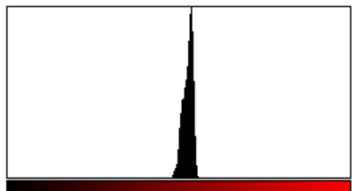


Count: 22500
Mean: 148.659
StdDev: 7.803
Min: 130
Max: 180
Mode: 140 (1068)

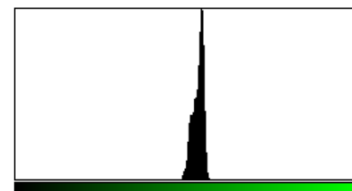


Count: 22500
Mean: 121.847
StdDev: 9.158
Min: 101
Max: 156
Mode: 125 (943)

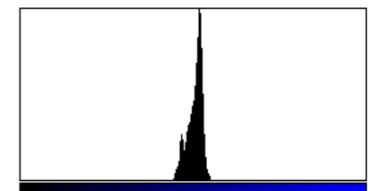
Patient #20247 Chip 1



Count: 22500
Mean: 134.291
StdDev: 3.727
Min: 121
Max: 143
Mode: 137 (2730)

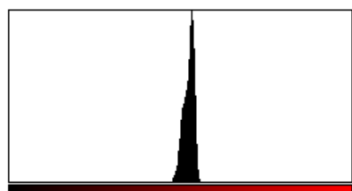


Count: 22500
Mean: 135.619
StdDev: 4.068
Min: 122
Max: 144
Mode: 138 (2685)

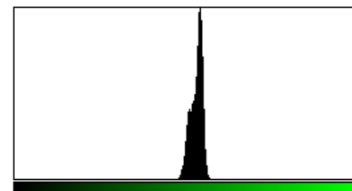


Count: 22500
Mean: 128.863
StdDev: 5.469
Min: 111
Max: 143
Mode: 132 (2355)

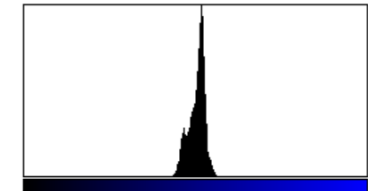
Patient #20247 Chip 2



Count: 22500
Mean: 133.823
StdDev: 3.998
Min: 120
Max: 144
Mode: 136 (2580)

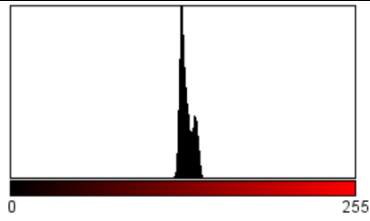


Count: 22500
Mean: 135.187
StdDev: 4.400
Min: 118
Max: 146
Mode: 138 (2460)

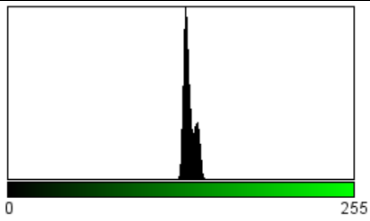


Count: 22500
Mean: 128.549
StdDev: 6.011
Min: 109
Max: 145
Mode: 132 (2160)

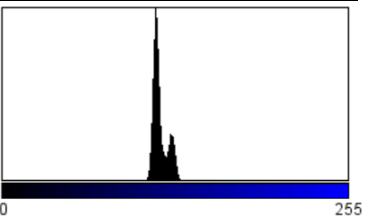
Patient #16701 Tubes



Count: 22500
Mean: 130.046
StdDev: 4.789
Min: 120
Max: 178
Mode: 127 (2650)

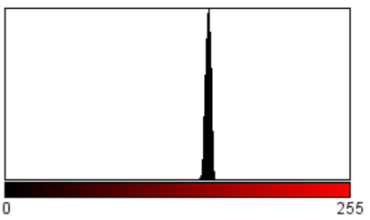


Count: 22500
Mean: 133.682
StdDev: 4.181
Min: 124
Max: 180
Mode: 131 (2937)

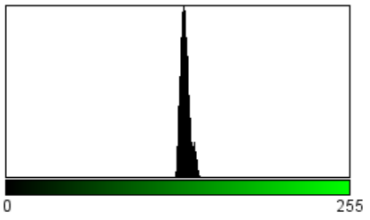


Count: 22500
Mean: 116.310
StdDev: 5.446
Min: 106
Max: 167
Mode: 113 (2866)

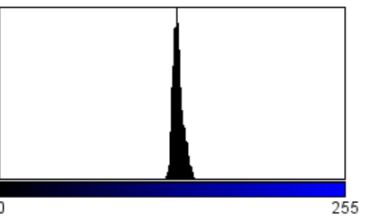
Patient #16701 Chip 1



Count: 22500
Mean: 150.393
StdDev: 2.086
Min: 143
Max: 156
Mode: 151 (3879)

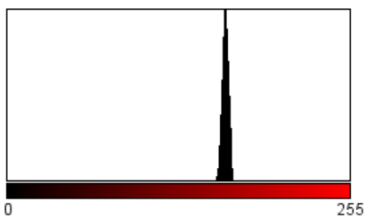


Count: 22500
Mean: 133.019
StdDev: 3.490
Min: 124
Max: 145
Mode: 132 (2726)

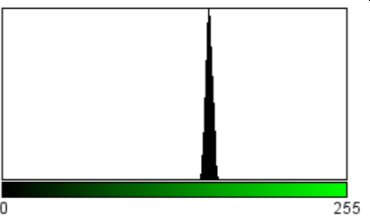


Count: 22500
Mean: 131.801
StdDev: 3.831
Min: 121
Max: 145
Mode: 131 (2678)

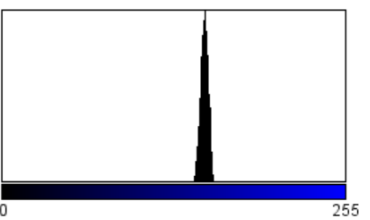
Patient #16701 Chip 2



Count: 22500
Mean: 162.646
StdDev: 2.452
Min: 152
Max: 169
Mode: 162 (3417)

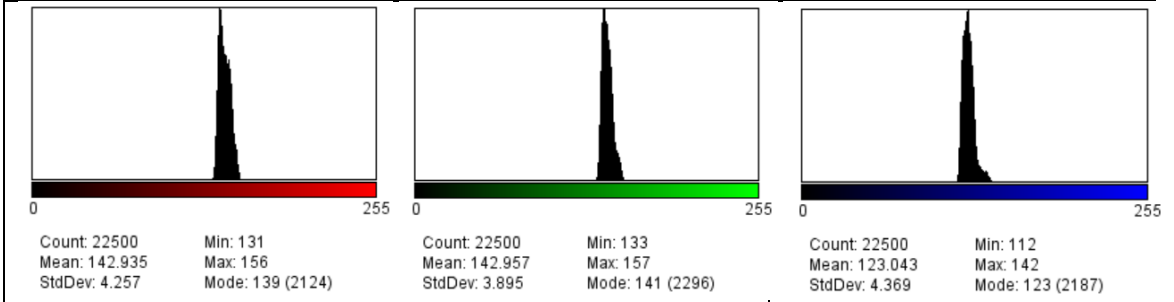


Count: 22500
Mean: 153.345
StdDev: 2.580
Min: 142
Max: 161
Mode: 153 (3342)

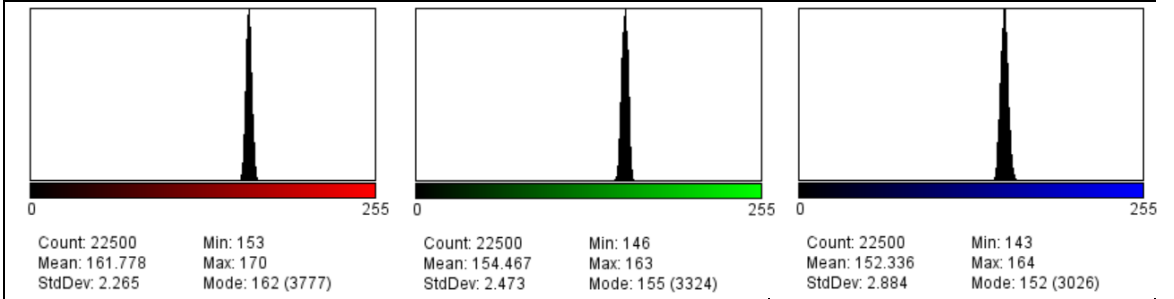


Count: 22500
Mean: 150.455
StdDev: 2.895
Min: 140
Max: 161
Mode: 151 (2996)

Patient #10439 Tubes



Patient #10439 Chip 1



Patient #10439 Chip 2

